Coordination Chemistry Reviews, 100 (1990) 363–402
Elsevier Science Publishers B.V., Amsterdam – Printed in The Netherlands

VIBRATIONAL SPECTRA OF DIOXYGEN ADDUCTS OF METAL CHELATE COMPOUNDS

KAZUO NAKAMOTO

Todd Wehr Chemistry Building, Marquette University, Milwaukee, WI 53233 (U.S.A.)

(Received 16 March 1989)

CONTENTS

ABBREVIATIONS

B	base
n-$BuNH_2$	*n*-butylamine
4-CNPy	4-cyanopyridine
1,2-DiMeIm	1,2-dimethylimidazole
3,4-DiMePy	3,4-dimethylpyridine
4-DMAPy	4-dimethylaminopyridine
Hb	hemoglobin
HRP	horse-radish peroxidase
Im	imidazole
J-en	*N*,*N*′-ethylene-bis(2,2-diacetylethylideneaminato) dianion (Fig. 1(B))

0010-8545/90/$14.00

M	metal
Mb	myoglobin
1-MeIm	1-methylimidazole
NADH	nicotinamide adenine dinucleotide
OEP	octaethylporphyrinato dianion (Fig. 1(A))
P or Por	porphyrinato anion
Pc	phthalocyanato anion
4-PhPy	4-phenylpyridine
γ-pic	γ-picoline
pip	piperidine
PPIXDME	protoporphyrin IX dimethyl ester dianion (Fig. 1(A))
py	pyridine

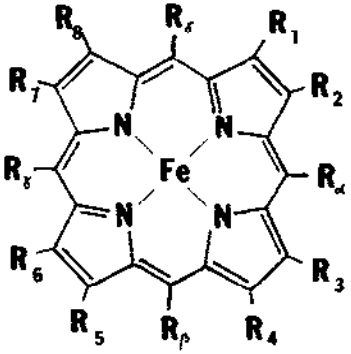

Fe(OEP): $R_1 \sim R_8 = C_2H_5$, $R_\alpha \sim R_\delta = H$

Fe(TMP): $R_\alpha \sim R_\delta$ = trimethylphenyl (mesityl), $R_1 \sim R_8 = H$

Fe(TPP): $R_\alpha \sim R_\delta$ = phenyl, $R_1 \sim R_8 = H$

Fe(PPIXDME): $R_1 = R_3 = R_5 = R_8 = CH_3$

$R_2 = R_4$ = vinyl

$R_6 = R_7$ = propionic acid

$R_\alpha \sim R_\delta = H$

(A)

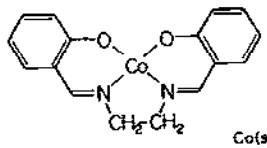

Co(salen)

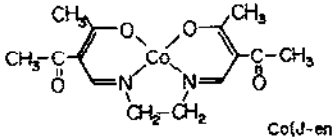

Co(J-en)

(B)

Fig. 1. Structures of porphyrins (A) and Schiff base complexes (B).

R	Raman
RR	resonance Raman
$T_{neo}PP$	*meso*-tetrakis[-*o*-(neopentylcarboxamido)phenyl]porphyrinato dianion
$T_{piv}PP$	*meso*-tetrakis[-*o*-(pivalamido)phenyl]porphyrinato dianion
TMP	tetramesitylporphyrinato dianion (Fig. 1(A))
TPP	tetraphenylporphyrinato dianion (Fig. 1(A))
salen	*N,N'*-ethylenebis(salicylideniminato) dianion (Fig. 1(B))

Greek symbols

δ	bending mode
ν	stretching mode
ν_a	antisymmetric stretching mode
ν_s	symmetric stretching mode

A. INTRODUCTION

Dioxygen (molecular oxygen) adducts of metal chelate compounds are highly important as modes of hemoglobin, myoglobin and cytochrome P-450 in their oxy states and as industrial catalysts in oxidation reactions of organic compounds. Many review articles [1–11] are available on various aspects of dioxygen adducts. The main objective of this article is to provide a comprehensive survey of the vibrational spectra of dioxygen adducts of metal chelate compounds with emphasis on the $\nu(O_2)$ and $\nu(M-O_2)$ or $\nu(M-O)$ vibrations.

The $M-O_2$ bond is formed by donation of electrons from the metal to the antibonding $2p\pi^*$ orbitals of dioxygen. Rudimentary MO theory predicts that the bond order decreases in the order O_2^+ (2.5) > O_2 (2.0) > O_2^- (1.5) > O_2^{2-} (1.0). As shown in Table 1, this results in an increase in the O–O bond distance, a decrease in the O–O bond energy and a downward shift of $\nu(O_2)$ in the same order. In fact, there are approximate linear

TABLE 1

Relationship between bond order, bond distance, bond energy [a] and O_2 stretching frequency

	Bond order	Bond distance (Å)	Bond energy (kcal mol^{-1})	$\nu(O_2)$ (cm^{-1})
O_2^+	2.5	1.123	149.4	1858
O_2 (triplet)	2.0	1.207	117.2	1555
$K[O_2^-]$	1.5	1.280	–	1108
$K_2[O_2^{2-}]$	1.0	1.49	48.8	762/746

[a] Values for the O–O distance and bond energy were taken from ref. 7.

relationships between the bond order and the other parameters mentioned above.

In the early stage of the vibrational studies, it was thought that all dioxygen adducts could be classified into two types: those which exhibit $\nu(O_2)$ in the 1200–1070 cm^{-1} region were called "superoxo" since the $\nu(O_2)$ bands of simple superoxides such as KO_2 are near 1100 cm^{-1} [12], and those which exhibit $\nu(O_2)$ in the 930–750 cm^{-1} region were called "peroxo" since simple peroxides such as K_2O_2 exhibit $\nu(O_2)$ at ca. 750 cm^{-1} [13]. As will be shown later, the $\nu(O_2)$ vibrations of metal chelate compounds vary continuously from 1300 to 700 cm^{-1}, depending on the nature of the metal ion and the in-plane and axial ligands. Thus it is not possible to draw a clear-cut borderline between the "superoxo" and "peroxo" adducts.

Structurally, dioxygen adducts are classified into three types:

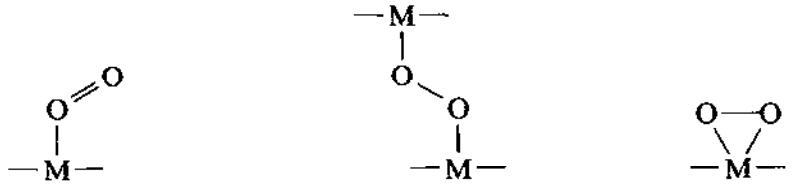

Although these structures are drawn for "base-free" adducts, "base-bound" adducts may be formed by the coordination of the base ligand to the vacant axial position.

Base-free end-on adducts of iron(II) and cobalt(II) chelates are extremely unstable and can be prepared only in low temperature gas matrices. Because of the low symmetry of the adducts, both $\nu(O_2)$ and $\nu(M-O_2)$ are expected to be IR as well as Raman active. These vibrations appear in the 1300–1200 cm^{-1} and 500–300 cm^{-1} regions respectively. When a base ligand coordinates to the axial position, the O–O bond is weakened and the $M-O_2$ bond is strengthened. As a result, $\nu(O_2)$ is lowered to the 1200–1100 cm^{-1} region and $\nu(M-O_2)$ is raised to the 600–500 cm^{-1} region. In some cases, the M–O–O bending, $\delta(MOO)$, has been observed in the 300–250 cm^{-1} region [14,15].

The six-coordinate base-bound adduct is most common. As shown in Fig. 2, $\nu(O_2)$ and $\nu(M-O_2)$ are governed by the nature of the central metal ion, the base ligand and the in-plane chelating ligand. Furthermore, these frequencies are influenced by the nature of the environment (solvent or cavity) surrounding the bound dioxygen. The effects of these factors on vibrational frequencies will be discussed in the following sections.

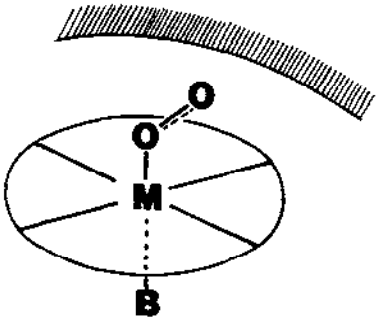

Fig. 2. Structure of "base-bound" end-on dioxygen adduct.

Bridging dioxygen adducts are well known for cobalt(III) ammine complexes. For example, $[(NH_3)_5Co(O_2^-)Co(NH_3)_5]Cl_5$ and $[(NH_3)_5Co(O_2^{2-})$-$Co(NH_3)_5]Cl_4$ exhibit $\nu(O_2)$ at 1122 cm^{-1} and 824 cm^{-1} respectively [16,17], and ν_s(Co–O) and ν_a(Co–O) in the 650–400 cm^{-1} region [16]. Since the Co–O–O–Co bridge is centrosymmetric, $\nu(O_2)$ and ν_s(Co–O) are Raman active while ν_a(Co–O) is IR active. Bridging dioxygen adducts are less common in metalloporphyrins and Schiff base complexes. Recently, the formation of an Fe–O–O–Fe intermediate during the oxidation process of iron(II) porphyrins was detected by resonance Raman (RR) spectroscopy [18]. Owing to its ideal geometry, anthracene-pillared dicobalt diporphyrin forms highly stable bridging adducts [19]. Schiff base complexes such as Co(salen) absorb dioxygen to form $[Co(salen)]_2O_2$ which contains the Co–O–O–Co bridge. Interestingly, its $\nu(O_2)$ (1011 cm^{-1}) is between the superoxo and peroxo ranges [20]. However, this frequency is lowered to 910–880 cm^{-1} when the base ligand coordinates to the axial positions [21].

The side-on structure is common among dioxygen adducts of metal atoms [12] and complexes of the second- and third-row transition metals such as molybdenum and tungsten. The $\nu(O_2)$ vibrations of the former scatter over a wide range from 1116 cm^{-1} (CsO_2) to 946 cm^{-1} (FeO_2) to 750 cm^{-1} (K_2O_2) [13], while those of the latter are concentrated in the 900–800 cm^{-1} region. These adducts also exhibit ν_s(M–O) and ν_a(M–O) in the low frequency region [22]. Under C_{2v} symmetry, all three vibrations are IR and Raman active. Side-on adducts are rare in metalloporphyrins. Their $\nu(O_2)$ are much lower than those of end-on adducts: $Mn(TPP)O_2$, 983 cm^{-1} [23,24]; and $[Fe(III)(OEP)(O_2^{2-})]^-$, 780 cm^{-1} [25].

In the following sections, the discussion is focused on the dioxygen adducts of metal chelate compounds of cobalt(II), iron(II) and manganese(II) because these are the most common and the most biologically important.

B. EXPERIMENTAL TECHNIQUES

(i) IR spectra

If the O_2 adduct is stable in solution at room temperature, the IR spectrum can be measured readily by using conventional liquid cells. If the O_2 adduct is stable only at low temperatures, a specially designed low temperature Dewar cell must be employed. As an example, the IR spectra of Fe(TPP)(pip)$_2$ (trace A), Fe(TPP)(pip)$^{16}O_2$ (trace B) and its $^{18}O_2$ analog (trace C) obtained in CH_2Cl_2 at $-70\,^\circ C$ [26] are shown in Fig. 3. The solvent bands have been subtracted in these spectra. The bands at 1157 and 1093 cm^{-1} can be assigned definitively to the $\nu(^{16}O_2)$ and $\nu(^{18}O_2)$ bands of Fe(TPP)(pip)O_2 respectively, because the magnitude of the isotopic shift (64 cm^{-1}) is in perfect agreement with that expected for a diatomic O–O vibrator.

If the O_2 adduct is obtained as crystals or as a film, conventional techniques used for solid samples (KBr pellets, Nujol mulls, films) are sufficient to measure the IR spectra. If cooling is necessary, a low temperature Dewar cell should be employed.

If the O_2 adduct is stable only below 100 K, the matrix co-condensation technique [12] may be used to obtain the IR spectra. The principle of this method is as follows: a sample of a metal chelate is vaporized from a Knudsen cell in a vacuum system (10^{-5}–10^{-6} Torr) and co-condensed with

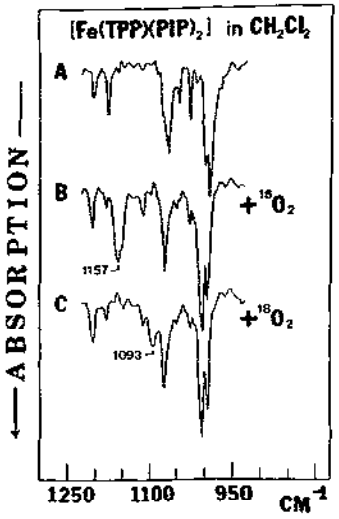

Fig. 3. The IR difference spectra in CH_2Cl_2 at ca. $-70\,^\circ C$ [26]: of: A, Fe(TPP)(pip)$_2$; B, Fe(TPP)(pip)$^{16}O_2$; C, Fe(TPP)(pip)$^{18}O_2$.

O_2 diluted in argon on a CsI window which is cooled to ca. 15 K by using a cryocooler. The spectra are then recorded by conventional methods [27–29]. If the metal chelate is air sensitive (e.g. Fe(II)(TPP)), its stable form (e.g. Fe(TPP)$(pip)_2$) is placed in the Knudsen cell and heated to an appropriate temperature to remove extra base ligands in the vacuum system. After complete dissociation of the base from the complex is confirmed, the co-condensation procedure described above is initiated [28,29].

(ii) Resonance Raman spectra

Dioxygen adducts of metalloporphyrins and Schiff base complexes are ideal for RR measurements because they have strong electronic absorption bands in the UV–visible region. Thus, it is possible to obtain high quality spectra with a small volume of a dilute solution or from a small sample area of a crystal surface or film if a proper resonance condition is employed. More importantly, it is possible to enhance only those vibrations localized within the chromophoric group if the exciting-line wavelength is chosen near that of the relevant chromophore (selectivity). As an example, consider a metalloporphyrin which exhibits three electronic transitions, α (or Q_0) and β (or Q_1) in the 500–600 nm region and Soret (or B) near 420 nm, all of which originate in the π–π^* transitions of the porphyrin core. Here β (or Q_1) is the vibronic band of α (or Q_0). According to theoretical treatments given elsewhere [30,31], the spectra obtained by Soret excitation consist of totally symmetric vibrations (A_{1g} under D_{4h} symmetry of the porphyrin core), whereas those obtained by α or β excitation are dominated by non-totally symmetric vibrations (B_{1g}, B_{2g} and A_{2g}). Axial ligand vibrations such as $\nu(O_2)$ and $\nu(M–O_2)$ can be resonance enhanced if the porphyrin π–π^* transition is coupled vibronically with the axial modes or if the excitation is carried out at the $M–O_2$ charge transfer (CT) transition which may be hidden under the strong Soret band. It should be noted that RR spectra of heme proteins thus obtained exhibit only porphyrin core (active site) vibrations without interference from those of the peptide backbone.

If the O_2 adduct is formed in solution, use of a rotating cell or a low temperature Dewar cell is recommended because local heating by the laser beam tends to decompose the O_2 adduct. In our laboratory, we developed the "mini-bulb" technique [32] which was employed to obtain most of the solution spectra quoted in this review. In this procedure a solution of a metal chelate (10^{-3}–10^{-4} mol l^{-1}) is first prepared with or without a base ligand in a small bulb (ca. 0.4 ml) using a standard vacuum line. After the solution is frozen by liquid N_2, a small amount of O_2 is added and the bulb is sealed off. This mini-bulb is attached to the front edge of the cold tip cooled by a cryocooler. The temperature of the bulb is controlled by the

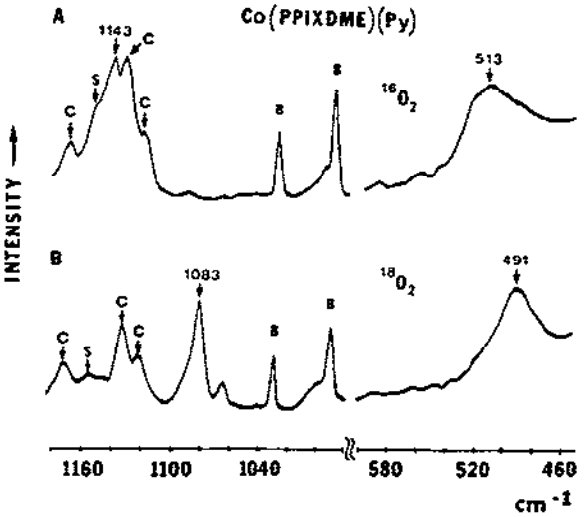

Fig. 4. RR spectra of Co(PPIXDME)(py)O_2 (A) and its $^{18}O_2$ analog (B) in CH_2Cl_2 at ca. −70 °C (457.9 nm excitation). S, C and B denote the solvent, complex and base respectively [33].

heater around the cooling unit, and can be estimated from the relative intensities of the Stokes and anti-Stokes lines of the solvent. This technique provides the following advantages.

(1) Only very small quantities of the sample and O_2 are required. This gives a considerable saving when expensive chemicals such as picket-fence porphyrins and $^{18}O_2$ gas are used.

(2) The temperature of the solution can be changed continuously over a wide range.

(3) The O_2 pressure can be varied from 1 to ca. 4 atm. Using this method, it is possible to increase the concentration of the O_2 adduct by lowering the temperature and by increasing the O_2 pressure in the bulb.

As an example, the RR spectra of Co(PPIXDME)(py)O_2 in CH_2Cl_2 obtained by this technique [33] are shown in Fig. 4. Although the spectra in the $\nu(O_2)$ region are complicated, the band at 1143 cm^{-1} can be assigned to $\nu(O_2)$ because only this band is shifted to 1083 cm^{-1} by $^{16}O_2/^{18}O_2$ substitution. However, the spectra in the $\nu(Co–O_2)$ region are simple; $\nu(Co–O_2)$ at 513 cm^{-1} is shifted to 491 cm^{-1} by $^{16}O_2/^{18}O_2$ substitution.

If the O_2 adduct is obtained as crystals or films, RR spectra should be measured by using the rotating-sample technique or by lowering the temperature to minimize the effect of local heating. If the O_2 adduct is stable only at cryogenic temperatures, the matrix co-condensation technique, similar to that used for IR spectroscopy, may be employed with slight modification. In

our laboratory, we developed the "laser-heated micro-oven" technique [34] to vaporize the metal complex and co-condense it with O_2 diluted in argon on a cold tip which is cooled to ca. 15 K with a cryocooler. The advantages of this technique are: (1) the same laser can be used for sample heating and spectral measurement; (2) very small amounts of samples (ca. 0.2 mg) are needed to measure the spectra; and (3) electronic and Raman spectra can be measured from the same sample area by changing the light source.

(iii) Isotope scrambling method

In the isotope scrambling method, the IR or RR spectra of dioxygen adducts are measured using an isotopic mixture of $^{16}O_2$, $^{16}O^{18}O$ and $^{18}O_2$ which can be obtained by electrical discharge of an $^{16}O_2/^{18}O_2$ mixture in a desired ratio. The final mixing ratio can be determined by measuring the intensities of the individual $\nu(O_2)$ vibrations in the 1600–1400 cm^{-1} region. The spectra thus obtained may be used to distinguish between the end-on and side-on structures since the former should exhibit a four-peak pattern (Fig. 5(A)), whereas the latter should show a three-peak pattern in the $\nu(O_2)$ region (Fig. 5(B)). In practice, however, the magnitude of the separation between the two central peaks in the former depends upon the M–O–O angle. Thus a single band may be observed if this angle is too small (less than 130°) [39]. In the $\nu(M–O_2)$ region, the end-on adduct exhibits two bands, one being an overlap of $\nu(M–^{16}O–^{16}O)$ and $\nu(M–^{16}O–^{18}O)$, and the other being an overlap of $\nu(M–^{18}O–^{16}O)$ and $\nu(M–^{18}O–^{18}O)$ [35]. The side-on structure can be recognized without isotope scrambling data because

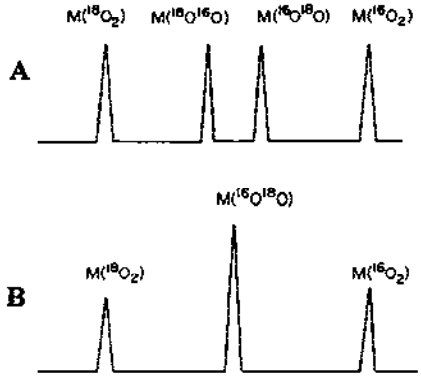

Fig. 5. Expected splitting patterns for scrambled dioxygen adducts ($^{16}O_2 : {}^{16}O^{18}O : {}^{18}O_2$ = 1 : 2 : 1): (A) end-on adduct; (B) side-on adduct.

it exhibits the ν_a(M–O) and ν_s(M–O) bands, both of which are isotope sensitive.

The isotope scrambling data are also important in interpreting the spectra in the $\nu(O_2)$ region. As will be shown in Section F, the RR spectra of the O_2 adducts of cobalt(II) porphyrins in the $\nu(O_2)$ region are extremely complicated because of vibrational coupling between $\nu(O_2)$ and the internal mode of the base ligand and/or solvent. In such a case, the $\nu(^{16}O-^{18}O)$ band can be used to confirm the presence of vibrational coupling and to estimate the unperturbed $\nu(O_2)$ value.

C. "BASE-FREE" DIOXYGEN ADDUCTS

As stated in Section A, coordination of the base ligand to the axial position of "base-free" O_2 adducts weakens the O–O bond and strengthens the M–O_2 bond via σ- or π-electron donation from the base to the dioxygen. The magnitude of the base-ligand effect may be estimated by comparing $\nu(O_2)$ and ν(M–O_2) with those of the corresponding "base-bound" adduct. Although most "base-free" O_2 adducts are unstable, they can be prepared by using the matrix co-condensation technique described in Section B.

The IR spectra of Fe(TPP) and its O_2 adducts obtained in argon and O_2–Ar matrices at ca. 15 K [29] are shown in Fig. 6. It can be seen that the co-condensation product of Fe(TPP) with $^{16}O_2$–Ar produces two new bands at 1195 and 1106 cm^{-1} (Fig. 6(B)) which are shifted to 1127 cm^{-1} and 1043 cm^{-1} respectively by $^{16}O_2/^{18}O_2$ substitution (Fig. 6(D)). As can be seen from the data in Table 2, this system is unique in that it exhibits two $\nu(O_2)$ bands in the same matrix. On the basis of several pieces of information given in ref. 29, the band at 1195 cm^{-1} was assigned to the end-on type and the band at 1106 cm^{-1} was attributed to the side-on type.

The $\nu(O_2)$ values of "base-free" O_2 adducts obtained in our laboratory are listed in Table 2 and several trends can readily be noted. (1) The $\nu(O_2)$ values of end-on adducts are higher than those of side-on adducts. (2) The $\nu(O_2)$ values follow the order cobalt(II) > iron(II) > manganese(II) in the porphyrin series. (3) The $\nu(O_2)$ values follow the order, Pc > TPP > salen in the Fe–chelate series. If $\nu(O_2)$ is regarded as a rough measure of the net negative charge on dioxygen [10], these results imply that the amount of negative charge on O_2 increases: (1) on going from the end-on to the side-on structure; (2) in the order cobalt(II) < iron(II) < manganese(II) (metal ion effect); and (3) in the order Pc < TPP < salen (in-plane ligand effect).

The initial attempt to obtain the RR spectra of Fe(TPP)O_2 in O_2 matrices led to unexpected results which turned out to be biologically important [39]. As shown in Fig. 7(A), a new band appears at 852 cm^{-1} when the matrix is irradiated by laser beam (406.7 nm). The intensity of this band is time

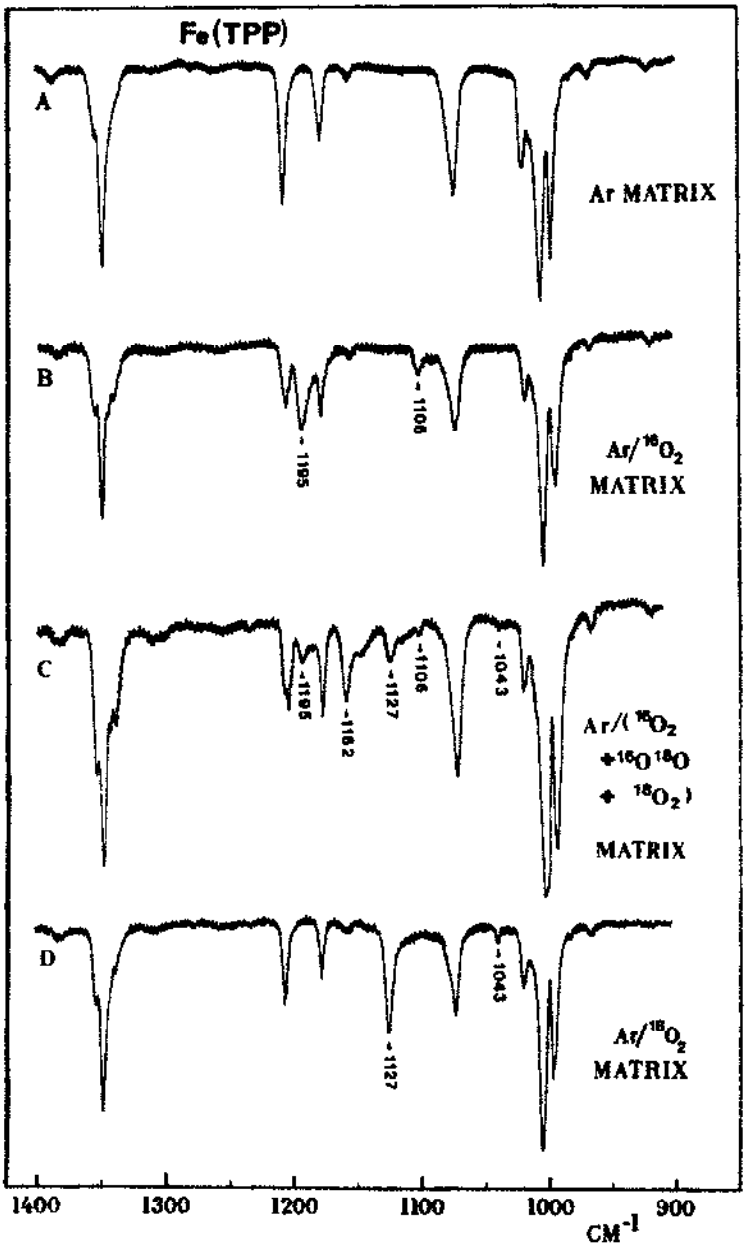

Fig. 6. The IR spectra at ca. 15 K [29] of: A, Fe(TPP); B, Fe(TPP) + $^{16}O_2$; C, Fe(TPP) + scrambled O_2; D, Fe(TPP) + $^{18}O_2$.

dependent, reaching the maximum after about 20 min. This band is shifted to 818 cm^{-1} by $^{16}O/^{18}O$ substitution (Fig. 7(B)) and similar experiments with scrambled O_2 produce two bands at 852 and 818 cm^{-1} (Fig. 7(C)).

TABLE 2

The $\nu(O_2)$ (cm^{-1}) (IR) of "base-free" O_2 adducts in low temperature matrices

Compound	Type	$\nu(^{16}O_2)$	$\nu(^{18}O_2)$	$\Delta\nu$	Ref.
$Co(TPP)O_2$	End-on	1278	1209	69	27
$Co(OEP)O_2$	End-on	1275	1202	73	36
$Co(J\text{-}en)O_2$	End-on	1260	1192	68	32
$Co(salen)O_2$	End-on	1235	1168	67	37
$[Co(salen)]_2O_2$ [a]	Bridging	1011	943	68	20
$Fe(TPP)O_2$	End-on	1195	1127	68	29
	Side-on	1106	1043	63	29
$Fe(OEP)O_2$	End-on	1190	1124	66	29
	Side-on	1104	1042	62	29
$Fe(Pc)O_2$	End-on	1207	1144	63	29
$Fe(salen)O_2$	Side-on	1106	1043	63	29
$[Fe(salen)]_2O_2$	Bridging	1001	943	58	38
$Mn(TPP)O_2$	Side-on	983	933	50	23
$Mn(OEP)O_2$	Side-on	(991) [b]	934	57 [b]	24
$Mn(Pc)O_2$	Side-on	992	935	57	24

[a] Solid state RR spectra. [b] Estimated value.

Both bands show upward shifts of 4 cm^{-1} on $^{NA}Fe/^{54}Fe$ substitution (broken lines in Figs. 7(A) and 7(B)). Here, ^{NA}Fe (natural abundance) contains 92% ^{56}Fe. These results definitely indicate that the new bands at 852 and 818 cm^{-1} are due to the $\nu(Fe{=}^{16}O)$ and $\nu(Fe{=}^{18}O)$ of ferryl-porphyrin, O=Fe(TPP), respectively, which is formed by the cleavage of the O–O bond of $Fe(TPP)O_2$ by laser irradiation. A more complete study including the high frequency region [40] showed that O=Fe(OEP) and O=Fe(salen) are also produced by laser irradiation of $Fe(OEP)O_2$ and $Fe(salen)O_2$ respectively, and that the iron atoms in these ferryl compounds are iron(IV) and low spin.

The biological significance of the above finding was later confirmed by RR studies on horse-radish peroxidase (HRP) [41–43]. The active site of this enzyme is similar to that of Hb and Mb (Section H). During the catalytic cycle of HRP, the intermediate species HRP-I and HRP-II are formed. Although these species were found to be an Fe(IV)–porphyrin π-cation radical and a low spin Fe(IV)–porphyrin respectively, it was not known whether the sixth ligands in these intermediates were hydroxyl or oxo until careful RR studies were carried out by using special sampling devices in conjunction with a multichannel detector. It was found that both intermediates contain the ferryl group and that the $\nu(Fe{=}O)$ bands of HRP-II and HRP-I are at 776 cm^{-1} (neutral pH) [41,42] and 737 cm^{-1} (neutral pH) [43] respectively.

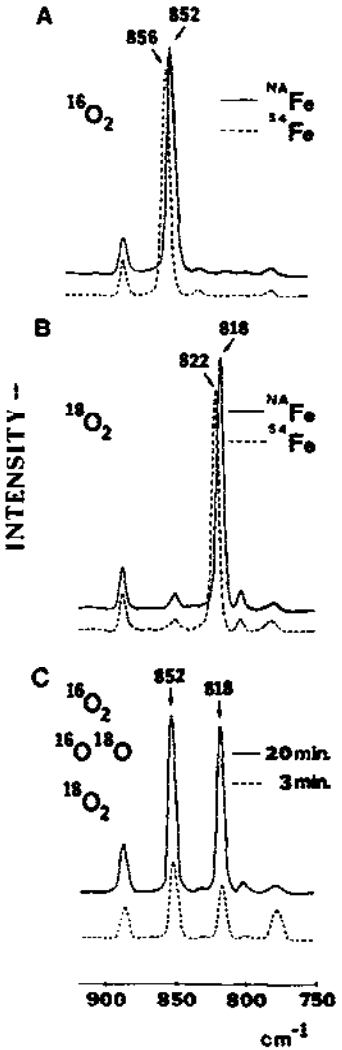

Fig. 7. The RR spectra of Fe(TPP) co-condensed with O_2 at ca. 15 K (406.7 nm excitation, 1–2 mW): A, ^{NA}Fe(TPP) with $^{16}O_2$ (———) and ^{54}Fe(TPP) with $^{16}O_2$ (- - - - -); B, ^{NA}Fe(TPP) with $^{18}O_2$ (———) and ^{54}Fe(TPP) with $^{18}O_2$ (- - - - -); C, ^{NA}Fe(TPP) with scrambled O_2 ($^{16}O_2$:$^{16}O^{18}O$:$^{18}O_2$ = 1:2:1). The solid and broken lines indicate the spectra after 20 min and 3 min of laser irradiation respectively [39].

Although laser irradiation of Fe(TPP)O_2 produces O=Fe(TPP), similar experiments with Fe(Pc)O_2 yield the RR spectra of Fe(Pc)O_2 without O–O bond cleavage [14]. As can be seen from Fig. 8, the RR spectra of Fe(Pc)O_2 exhibit two oxygen-isotope-sensitive bands below 500 cm^{-1}. Although the first band near 488 cm^{-1} is hidden under the strong Pc band at 486 cm^{-1}

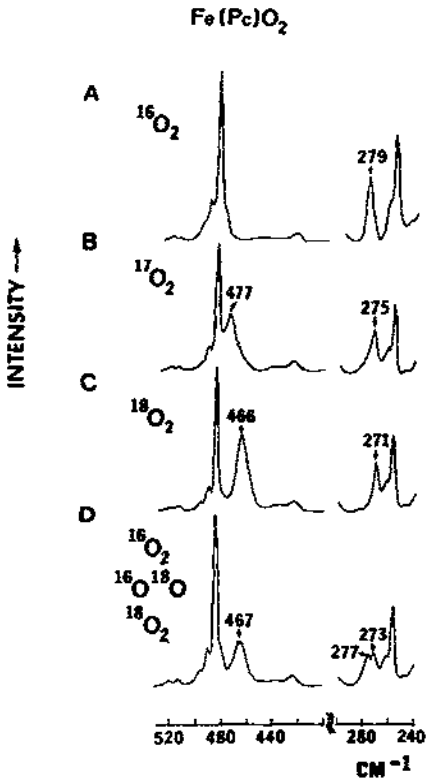

Fig. 8. The RR spectra of $Fe(Pc)O_2$ in O_2 matrices at ca. 15 K (676.4 nm excitation, ca. 10 mW). The $^{17}O_2$ and $^{18}O_2$ gases used were 77% and 98% pure respectively [14].

(Fig. 8(A)), it is shifted to 477 cm^{-1} (Fig. 8(B)) and 466 cm^{-1} (Fig. 8(C)) respectively by $^{16}O_2/^{17}O_2$ and $^{16}O_2/^{18}O_2$ substitutions. The second band at 279 cm^{-1} is shifted to 275 cm^{-1} and 271 cm^{-1} respectively by the same substitutions. The O_2 adduct with scrambled dioxygen exhibits two bands at 277 and 273 cm^{-1} (Fig. 8(D)). On the basis of normal-coordinate calculations on a bent Fe–O–O model, these two bands have been assigned to $\nu(Fe–O_2)$ and $\delta(FeOO)$ respectively, which are slightly coupled to each other [14]. This is one of the rare examples for which the M–O–O bending mode has been observed.

The RR spectra of $Fe(TPP)O_2$ in dioxygen matrices can be obtained if local heating due to laser irradiation is minimized by using the line-focusing technique. The RR spectra of co-condensed products of Fe(TPP) with $^{16}O_2$ (trace A), $^{18}O_2$ (trace B) and scrambled dioxygen ($^{16}O_2 : {}^{16}O^{18}O : {}^{18}O_2 \approx 1:2:1$, trace C) [44] are shown in Fig. 9. In agreement with the IR results discussed previously, the $\nu(^{16}O_2)$ and $\nu(^{18}O_2)$ bands of the end-on type adducts were observed at 1195 cm^{-1} and 1129 cm^{-1} respectively. The $\nu(O_2)$

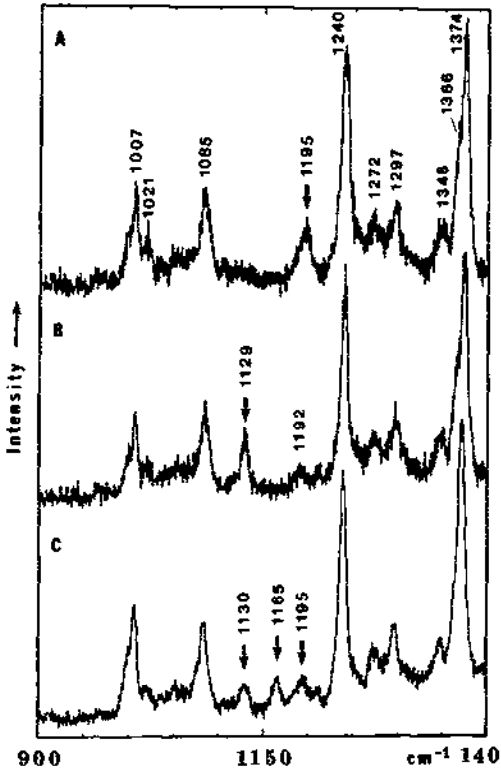

Fig. 9. The RR spectra (high frequency region) of the co-condensation products of Fe(TPP) with $^{16}O_2$ (A), $^{18}O_2$ (B) and scrambled O_2 ($^{16}O_2$:$^{16}O^{18}O$:$^{18}O_2$ = 1:2:1) (C) at ca. 25 K (406.7 nm excitation) [44].

bands of the side-on type adducts were not observed in this case owing to their low concentration relative to the end-on adducts. It has been tacitly assumed that $\nu(O_2)$ of heme proteins and their model compounds cannot be resonance enhanced unless the axial position *trans* to dioxygen is occupied by the thiolate ligand (Section H). Such an assumption must be re-examined in the light of these observations.

The RR spectra of Fe(TPP)O_2 in the low frequency region [44] are given in Fig. 10. It can be seen that the bands at 853 and 509 cm^{-1} (Fig. 10(A)) are shifted to 819 cm^{-1} and 487 cm^{-1} respectively by $^{16}O_2/^{18}O_2$ substitution (Fig. 10(B)) and that the adduct obtained with scrambled dioxygen exhibits both these bands with almost equal intensities (Fig. 10(C)). As discussed earlier, the bands at 853 and 819 cm^{-1} are due to O=Fe(TPP) and its ^{18}O analog respectively, which are produced by laser photolysis of the corresponding O_2 adducts. The newly observed bands at 509 and 487 cm^{-1} are assigned to the $\nu(Fe–O_2)$ band of "base-free" Fe(TPP)O_2 and its $^{18}O_2$

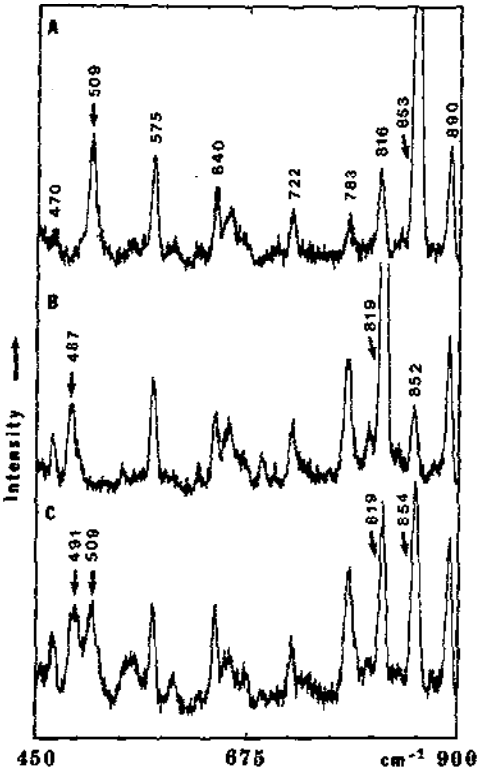

Fig. 10. The RR spectra (low frequency region) of the co-condensation products of Fe(TPP) with $^{16}O_2$ (A), $^{18}O_2$ (B) and scrambled dioxygen (C) at ca. 25 K (406.7 nm excitation) [44].

analog respectively, in accordance with the expected isotopic shift. These frequencies are considerably lower than those of six-coordinate, "base-bound" adducts (Section D) because the Fe–O_2 bond in the "base-free" adducts is much weaker due to the absence of electron donation from the base ligand. The ν(Fe=O) band at 853 cm^{-1} becomes stronger while the $\nu(O_2)$ band at 1195 cm^{-1} and the ν(Fe–O_2) band at 509 cm^{-1} become weaker as the laser power is increased or the irradiation time is lengthened. These results provide direct support for the mechanism that, in O_2 matrices, ferrylporphyrins are formed by the cleavage of the O–O bond of the end-on adducts.

D. "BASE-BOUND" DIOXYGEN ADDUCTS

The $\nu(O_2)$ bands of "base-free" adducts are shifted markedly to lower frequencies when base ligands coordinate to the axial position. For example, the $\nu(O_2)$ band of Co(TPP)O_2 (1278 cm^{-1}) is shifted down to 1144 cm^{-1}

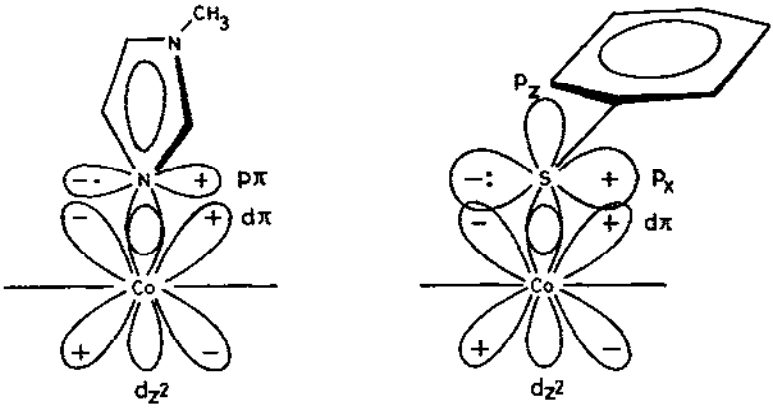

Fig. 11. Bonding schemes of 1-methylimidazole (A) and benzenethiolate (B) to cobalt(II) porphyrin. The horizontal line points to the direction of the porphyrin ring plane [45].

when 1-MeIm coordinates to the axial position [33]. Similar shifts are observed on going from Co(J-en)O_2 (1260 cm^{-1}) to Co(J-en)(py)O_2 (1143 cm^{-1}) [32], and from $[Co(salen)]_2O_2$ (1011 cm^{-1}) [20] to $[Co(salen)(py)]_2O_2$ (888 cm^{-1}) [21]. Evidently electron donation from the base to dioxygen is responsible for the observed downward shift. As shown in Fig. 11(A), the first step of this electron donation occurs from the base to the metal via σ and/or π overlap. This is followed by the second step in which the extra electron density thus produced on the metal is transmitted to dioxygen via σ and/or π overlap [45]. In both cases, the π overlap is dependent upon the orientation of the base ligand plane or the M–O–O plane with respect to that of the metal π-orbitals. In the following, we consider only the first step because we are interested in the effect of the base ligand. Except for some "protected" porphyrins (Section G), electron donation via the second step does not differ among metal chelate compounds.

A series of values of $\nu(O_2)$ of Co(TPP-d_8)(B)O_2-type compounds in which the pK_a of the py derivative is varied from 1.9 to 9.7 [46] is given in Table 3. The $\nu(O_2)$ values of these compounds are plotted vs. pK_a in Fig. 12. If the pK_a value is regarded as a rough measure of σ donation, these results suggest that $\nu(O_2)$ is governed largely by σ donation and that the effect of π donation is relatively small and fairly constant among the bases studied.

The $\nu(O_2)$ band is shifted markedly to lower frequency when a thiolate ligand such as $SC_6H_5^-$ coordinates to the metal. For example, $\nu(O_2)$ of Ⓚ[Co(TPP)(SC_6H_5)O_2] (Ⓚ = potassium 18-crown-6 ether) in CH_2Cl_2 is 21 cm^{-1} lower than that of Co(TPP)(py)O_2 in the same solvent [45]. The

TABLE 3

The $\nu(O_2)$ values of $Co(TPP\text{-}d_8)(B)O_2$ containing a series of base ligands (in toluene or toluene-d_8) [46]

Point [a]	Base ligand	pK_a	$\nu(O_2)$ (cm^{-1})
1	4-Dimethylaminopyridine	9.70	1151
2	2,4,6-Trimethylpyridine	7.43	1156
3	3,4-Dimethylpyridine	6.46	1157
4	4-Phenylpyridine	5.55	1158
5	Pyridine	5.25	1160
6	2-Formylpyridine	3.80	1162
7	3-Acetylpyridine	3.18	1163
8	4-Cyanopyridine	1.90	1167

[a] Refer to Fig. 12.

pK_a of $SC_6H_5^-$ (6.5) does not differ appreciably from that of py (5.25). Thus the observed shift must be attributed largely to an increase in π donation. The π donation by the $SC_6H_5^-$ ion is promoted by two factors: (1) as shown in Fig. 11(B), extra lone-pair electrons reside in the p_x orbital of the sulfur atom; and (2) the thiolate ion in TPP complexes tends to take an orientation which maximizes the p_x–d_π (metal) overlap and minimizes the steric repulsion from the *meso*-phenyl groups. The biological significance of thiolate coordination is discussed in Section H.

"Base-bound" dioxygen adducts are common among metal complexes of iron(II) and cobalt(II). The $\nu(O_2)$ of iron(II) porphyrins and those of the

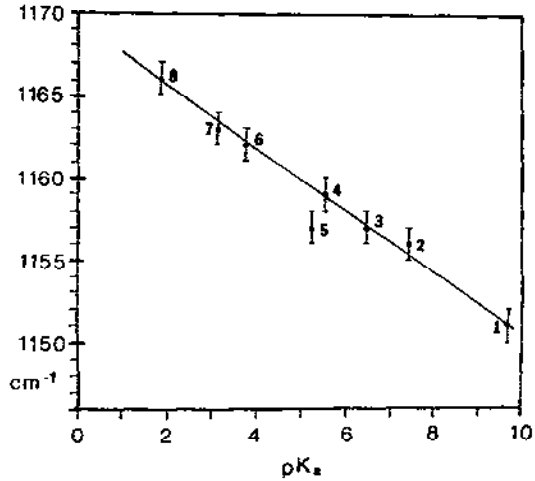

Fig. 12. Effect of ligand basicity on $\nu(O_2)$. For numbering, see Table 3 [46].

TABLE 4

The $\nu(O_2)$ (cm^{-1}) values of iron and cobalt porphyrins

Compound	Method	Solvent	$\nu(^{16}O_2)$	$\nu(^{18}O_2)$	$\Delta\nu(O_2)$ [a]	$\Delta\nu(M)$ [b] $\nu(^{16}O_2)$	$\Delta\nu(M)$ [b] $\nu(^{18}O_2)$	Ref.
$Fe(T_{piv}PP)(1,2\text{-}Me_2Im)O_2$	IR	C_6H_6	1159	1093	66	6	5	8, 47
$Co(T_{piv}PP)(1,2\text{-}Me_2Im)O_2$	RR	C_6H_6	1153 [c]	1088	65			26
$[Fe(T_{piv}PP)(SC_6HF_4)O_2]^-$	RR	C_6H_5Cl	1140	1080	60	13–14	16–20	48
	IR	C_6H_5F	1139	1076	63			49
$[Co(T_{piv}PP)(SC_6HF_4)O_2]^-$	IR	Solid [d]	1126	1060	66			50
Fe(TPP)(pip)O_2	IR	CH_2Cl_2	1157	1093	64	15	15	26
Co(TPP)(pip)O_2	RR	CH_2Cl_2	1142	1078	64			26
Co(TPP)(py)O_2	RR	CH_2Cl_2	1144	1084	60			33, 51
Co(TPP)(pip)O_2	RR	$C_6H_5CH_3$	1154	1092	62			26

[a] Oxygen isotope shift, $\nu(^{16}O_2)-\nu(^{18}O_2)$. [b] Metal-ion effect, $\nu(O_2, Fe)-\nu(O_2, Co)$. [c] Average of two frequencies observed at 1159 and 1147 cm^{-1} (see Section G). [d] This compound is too unstable to measure in chlorobenzene (see ref. 42).

corresponding cobalt(II) porphyrins [26] are compared in Table 4. It can be seen that both $\nu(^{16}O_2)$ and $\nu(^{18}O_2)$ shift consistently to lower frequencies on going from iron(II) to cobalt(II) porphyrins, although the magnitude of the shift depends upon the nature of the porphyrin, base ligand and isotopic oxygen involved. The $\nu(M-O_2)$ observed for two pairs of iron(II) and cobalt(II) porphyrins are summarized in Table 5. In this case, $\nu(M-O_2)$ is shifted to lower frequency by 51–66 cm^{-1} on going from iron(II) to cobalt(II) porphyrin. A somewhat smaller metal-ion effect is seen for the

TABLE 5

The $\nu(M-O_2)$ (cm^{-1}) values of iron and cobalt porphyrins [a]

Compound	Solvent	$\nu(M-^{16}O_2)$	$\nu(M-^{18}O_2)$	$\Delta\nu(O_2)$ [b]	$\Delta\nu(M)$ [c] $^{16}O_2$	$\Delta\nu(M)$ [c] $^{18}O_2$	Ref.
$Fe(T_{piv}PP)(N\text{-}MeIm)O_2$	CH_2Cl_2	568	545	23	51	51	52
$Co(T_{piv}PP)(N\text{-}Me_2Im)O_2$	CH_2Cl_2	517	494	23			26
$Co(T_{piv}PP)(N\text{-}MeIm)O_2$	C_6H_6	516	494	22			53
Fe(TPP)(pip)O_2	$C_6H_5CH_3$	575	551	24	66	62	26
Co(TPP)(pip)O_2	$C_6H_5CH_3$	509	489	20			26
Co(TPP)(pip)O_2	CH_2Cl_2	518	496	22			26
Co(TPP)(py)O_2	CH_2Cl_2	519	498	21			33, 51

[a] All frequencies determined by RR spectroscopy. [b] Oxygen isotope shift, $\nu(M-^{16}O_2)-\nu(M-^{18}O_2)$. [c] Metal-ion effect, $\nu(Fe-O_2)-\nu(Co-O_2)$, obtained in the same solvent. [d] Ref. 26.

pair, HbO_2 (567 cm^{-1}) [54] and cobalt(II)-reconstituted HbO_2 (537 cm^{-1}) [55].

In the preceding section, the $\nu(O_2)$ modes of "base-free" O_2 adducts were discussed. In that case, the $\nu(O_2)$ modes of cobalt(II) complexes are always higher than those of the corresponding iron(II) complexes (Table 2). As can be seen from the data in Table 4, the opposite trend prevails for "base-bound" O_2 adducts. The difference between these two cases may be accounted for in terms of the following bonding schemes:

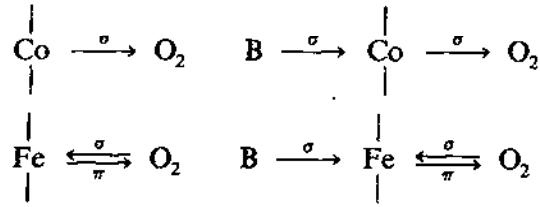

When the O_2 is bound to Co(II)(d^7), the Co–O_2 bond is formed mainly by σ donation from Co(d_{z^2}) to the antibonding $O_2(\pi_g^*)$ orbital (i.e. Co(III)–O_2^-) [57,58]. In the case of Fe(II)(d^6), however, the Fe–O_2 bond is formed by σ donation from $O_2(\pi_g^*)$ to Fe(d_{z^2}) which is counteracted by π donation in the opposite direction [52,57]. This process would strengthen the Fe–O_2 bond and weaken the O–O bond relative to those of the corresponding cobalt(II) complex. In fact, ν(Fe–O_2) of Fe(TPP)O_2 (509 cm^{-1}) [44] lies much higher than ν(Co–O_2) of Co(TPP)O_2 (345 cm^{-1}) [27]. In "base-bound" cobalt(II) complexes, σ donation from the base ligand causes a marked increase in the negative charge on O_2, thus lowering $\nu(O_2)$ from 1278 cm^{-1} (Co(TPP)O_2) to 1144 cm^{-1} (Co(TPP)(1-MeIm)O_2). However, the base-ligand effect is much smaller in the iron(II) complexes because σ donation from the base is opposed by σ donation from O_2. Thus the O_2 in the iron(II) complexes would be less negative than those in the cobalt(II) complexes. This is reflected in the trend $\nu(O_2)_{Fe} > \nu(O_2)_{Co}$, as seen in Table 4. In "base-free" as well as in "base-bound" complexes, however, ν(Fe–O_2) is always higher than ν(Co–O_2) due to the multiple-bond character of the former bond. This is clearly demonstrated by the data in Table 5.

E. SOLUTION EQUILIBRIA OF DIOXYGEN ADDUCTS

When a Schiff base complex, Co(J-en), dissolved in CH_2Cl_2 binds dioxygen in the presence of py, the following equilibria are established:

$$\text{Co(J-en)py} + O_2 \overset{K_1}{\rightleftharpoons} \text{Co(J-en)(py)}O_2 \qquad (1)$$

$$\text{Co(J-en)(py)}O_2 + \text{Co(J-en)(py)} \overset{K_2}{\rightleftharpoons} [\text{Co(J-en)(py)}]_2O_2 \qquad (2)$$

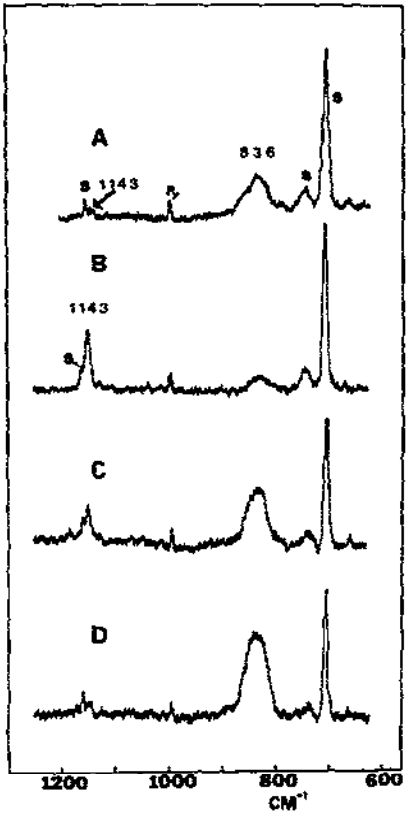

Fig. 13. The RR spectra of Co(J-en) in CH_2Cl_2 containing 3% pyridine which were saturated with O_2 at various O_2 pressures and temperatures (580 nm excitation): A, 1 atm, −78° C; B, ca. 3 atm, −78° C; C, ca. 3 atm, −30° C; D, ca. 3 atm, +20° C. S and py denote the solvent and pyridine bands respectively [32].

The RR spectrum of this solution under 1 atm O_2 pressure at −78° C [32] is shown in Fig. 13(A). The bands at 1143 and 836 cm^{-1} are shifted to 1081 cm^{-1} and 785 cm^{-1} respectively by $^{16}O_2/^{18}O_2$ substitution. The band at 1143 cm^{-1} is assigned to the 1 : 1 adduct, [Co(J-en)(py)O_2] because this frequency is typical of a six-coordinate base-bound adduct (Table 4). However, the band at 836 cm^{-1} is assigned to the 1 : 2 adduct [Co(J-en)(py)]$_2O_2$ because its $\nu(O_2)$ is characteristic of cobalt(III) peroxo-bridged complexes [21]. Similar solution equilibria have been found by RR studies of Co(salen) [58] and its derivatives [59].

Trace B in Fig. 13 [32] was obtained by increasing the O_2 pressure to ca. 3 atm while maintaining the same temperature (−78° C). It is seen that the 1 : 1 adduct peak becomes stronger while the 1 : 2 adduct peak becomes weaker. Namely, formation of the 1 : 1 adduct is favored at higher O_2

pressure. This is anticipated from equilibrium (1) as well as from equilibrium (3):

$$[\text{Co(J-en)(py)}]_2\text{O}_2 + \text{O}_2 \overset{K_1/K_2}{\rightleftharpoons} 2[\text{Co(J-en)(py)O}_2] \quad (3)$$

Figures 13(C) and 13(D) show the RR spectra of the same solution at $-30\,^\circ$C and $+20\,^\circ$C respectively. It is seen that the 1 : 1 adduct peak at 1143 cm^{-1} becomes weaker as the temperature is raised from -80 to $+20\,^\circ$C. Thus the 1 : 2 adduct is favored at higher temperature. The observed spectral changes are reversible within this temperature range. Although the O_2 pressure in the mini-bulb (Section B) used for these experiments is increased by raising the temperature, this pressure effect (seen in Figs. 13(A) and 13(B)) is not sufficient to offset the temperature effect.

The effect of solvent polarity can also be studied by comparing the RR spectra obtained in different solvents. These experiments show that the 1 : 1 adduct is stabilized in a polar solvent such as CH_3CN (3.97 D), whereas the 1 : 2 adduct is stabilized in a less polar solvent such as CH_2Cl_2 (1.54 D). In general, the Co(II)–O_2 bond is regarded as a being of the polar superoxo type [Co(III)–O_2^-] [7,56], which means that its formation from the less polar reactants is enhanced by polar solvents. The opposite trend is expected for the 1 : 2 adduct because the two Co(III)–O_2^- moments cancel each other, resulting in a small overall polarity.

The upper traces in Fig. 14 [32] show the electronic spectra of Co(J-en) in CH_3CN containing *n*-$BuNH_2$ saturated with N_2 and O_2 at $-35\,^\circ$C. It is seen that two new bands emerge at ca. 610 and 550 nm upon oxygenation of the solution. The lower traces in Fig. 14 show the RR excitation profiles of the $\nu(O_2)$ of the 1 : 1 adduct at 1143 cm^{-1} and the 1 : 2 adduct at 830 cm^{-1} obtained under similar experimental conditions. The former exhibits a maximum at ca. 550 nm, whereas the latter shows a maximum at ca. 610 nm with a weak shoulder in the 520–500 nm region. These results suggest that the electronic bands at ca. 550 and 610 nm are due to the Co–O_2 CT transitions of the 1 : 1 and 1 : 2 adducts respectively. Thus RR excitation profile studies are useful in locating the Co–O_2 CT transitions in poorly resolved electronic spectra.

In general, the oxidation process of iron(II) porphyrins proceeds via the following intermediates [60]:

$$\underset{\textbf{A}}{\text{PFe}} \xrightarrow{O_2} \underset{\textbf{B}}{\text{PFe—O}_2} \xrightarrow{\text{PFe}} \underset{\textbf{C}}{\text{PFe—O—O—FeP}} \longrightarrow$$

$$\underset{\textbf{D}}{\text{PFe=O}} \xrightarrow{\text{PFe}} \underset{\textbf{E}}{\text{PFe—O—FeP}}$$

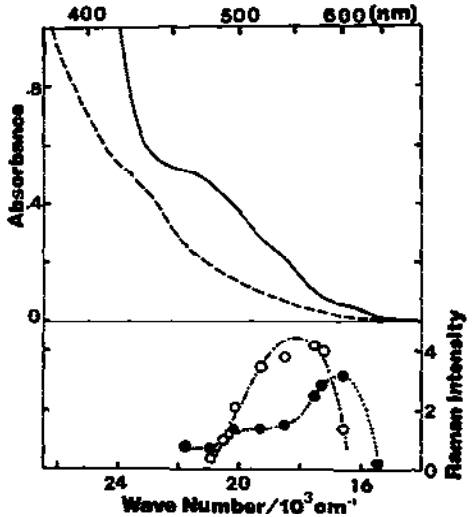

Fig. 14. The electronic spectra and excitation profiles of Co(J-en)(*n*-BuNH$_2$)O$_2$ and [Co(J-en)(*n*-BuNH$_2$)]$_2$O$_2$ in CH$_3$CN at −35°C. Upper curves: electronic spectra under N_2 (———) and O_2 (- - - - - -) atmospheres (2×10^{-4} mol l^{-1} with respect to Co(J-en). Lower curves: excitation profiles: (○) $\nu(O_2)$ of the 1:1 adduct, (●) $\nu(O_2)$ of the 1:2 adduct (10^{-2} mol l^{-1} with respect to Co(J-en)) [32].

As shown in Section C, the IR and RR spectra of **B** and the RR spectra of **D** have been obtained in low temperature gas matrices. Vibrational spectra of the stable final product, **E**, are well documented [61,62]. The existence of **C** in toluene at low temperatures was first confirmed by ^{1}H NMR spectroscopy [60]. As shown below, the presence of an equilibrium between **C** and **D** in toluene solution can be detected by using RR spectroscopy [18].

The RR spectra of Fe(TMP) measured at −78°C in toluene saturated with $^{16}O_2$ and $^{18}O_2$ are shown in Figs. 15(A) and 15(B) respectively. The RR spectra of the same solutions at −46°C are shown in Figs. 15(B) and 15(D). It can be seen that the bands at 845 (trace A) and 812 cm^{-1} (trace C) become stronger while those at 574 (trace A) and 543 cm^{-1} (trace C) disappear almost completely when the temperature is raised from −78 to −46°C. As discussed in Section C, the bands at 845 and 812 cm^{-1} are due to ν(Fe=O) of O=Fe(TMP) and its ^{18}O analog respectively. The newly observed bands at 574 and 547 cm^{-1} are assigned to ν_s(Fe–O) of the bridging species **C** and its $^{18}O_2$ analog respectively, on the basis of evidence obtained from ^{1}H NMR, UV–visible and RR spectral studies [18]. Apparently the bridging adduct is too unstable to remain at −46°C.

The bridging adduct can be stabilized considerably if a pillared dicobalt cofacial diporphyrin, such as that shown in Fig. 16 (Co–Co complex), is employed. The RR spectra at −80°C of the Co–Co complex in CH_2Cl_2

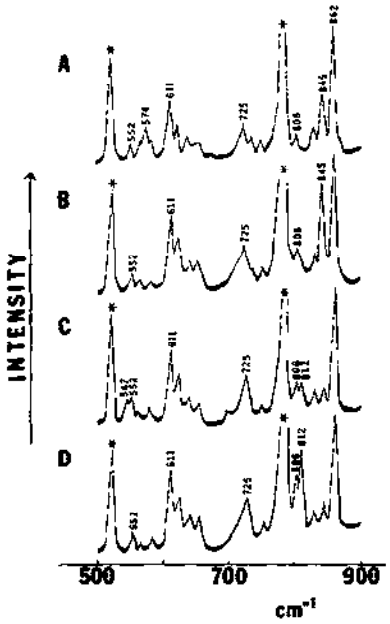

Fig. 15. The RR spectra of Fe(TMP) in toluene saturated with O_2: A, $^{16}O_2$ at $-78°C$; B, $^{16}O_2$ at $-46°C$; C, $^{18}O_2$ at $-78°C$; D, $^{18}O_2$ at $-46°C$. The asterisk denotes the solvent band [18].

containing 4-DMAPy saturated with $^{16}O_2$ and $^{18}O_2$ are shown in Figs. 17(A) and 17(B) [19]. It can be seen that the $^{16}O_2$ solution exhibits two $\nu(O_2)$ bands at 1139 and 1098 cm^{-1} which are shifted to 1081 cm^{-1} and 1039 cm^{-1} respectively by $^{16}O_2/^{18}O_2$ substitution. In the low frequency region, the $^{16}O_2$ solution exhibits two bands at 625 and 514 cm^{-1}, which are shifted to 597 cm^{-1} and 488 cm^{-1} respectively by $^{16}O_2/^{18}O_2$ substitution. When the solution is warmed to room temperature, the bands at 1139 (1081) and 514 (488) cm^{-1} disappear and the band at 1098 (1039) cm^{-1} becomes

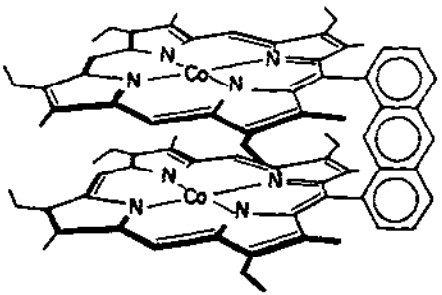

Fig. 16. The structure of Co–Co anthryldiporphyrin.

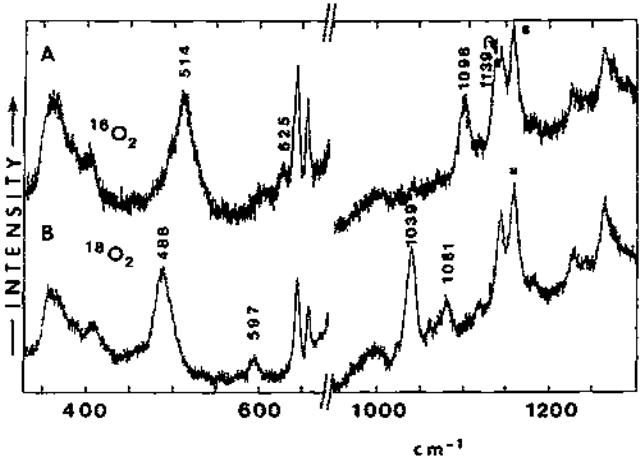

Fig. 17. The RR spectra of the dioxygen adducts of the Co–Co complex in CH_2Cl_2 containing 4-DMAPy at −80 °C (457.9 nm excitation) [19]: A, $^{16}O_2$; B, $^{18}O_2$. S denotes the solvent band.

stronger. Here the numeral in parentheses indicates the frequency of the $^{18}O_2$ adduct. The O_2 adduct stable at low temperature is characterized by $\nu(O_2)$ at 1139 (1081) cm^{-1} and ν(Co–O_2) at 514 (488) cm^{-1}, which are typical of a six-coordinate base-bound O_2 adduct, whereas the O_2 adduct stable at room temperature is characterized by $\nu(O_2)$ at 1098 (1039) cm^{-1} and ν_s(Co–O) at 625 (597) cm^{-1}, which originate in the superoxo bridging structure. Figure 18(A) shows the process of this oxidation; the broken line indicates the side-view of the inclined anthracene ring. Apparently, 4-DMAPy is too large to enter the interporphyrin cavity.

If similar experiments are carried out with a small base such as γ-pic, the bands characteristic of the bridging adduct do not appear. However, spectra similar to those shown in Fig. 17 are obtained if the Co–Co complex solution is first saturated with O_2 and the base ligand is then added. This peculiar phenomenon can be explained by the reaction schemes shown in Figs. 18(B) and 18(C). Namely, if added first, a small base ligand enters the interporphyrin cavity, thus blocking the formation of the Co–O–O–Co bridge. In the case of a large base such as 4-DMAPy, the order of adding the base and O_2 is not critical because it cannot slip into the cavity.

F. VIBRATIONAL COUPLING

The RR spectrum of Co(TPP-d_8)(py)O_2 exhibits a single $\nu(O_2)$ band at 1143 cm^{-1} in CH_2Cl_2 [33]. As shown in Fig. 19(A), this band becomes a doublet (1155 and 1139 cm^{-1}) when 1,2-DiMeIm is employed as the base

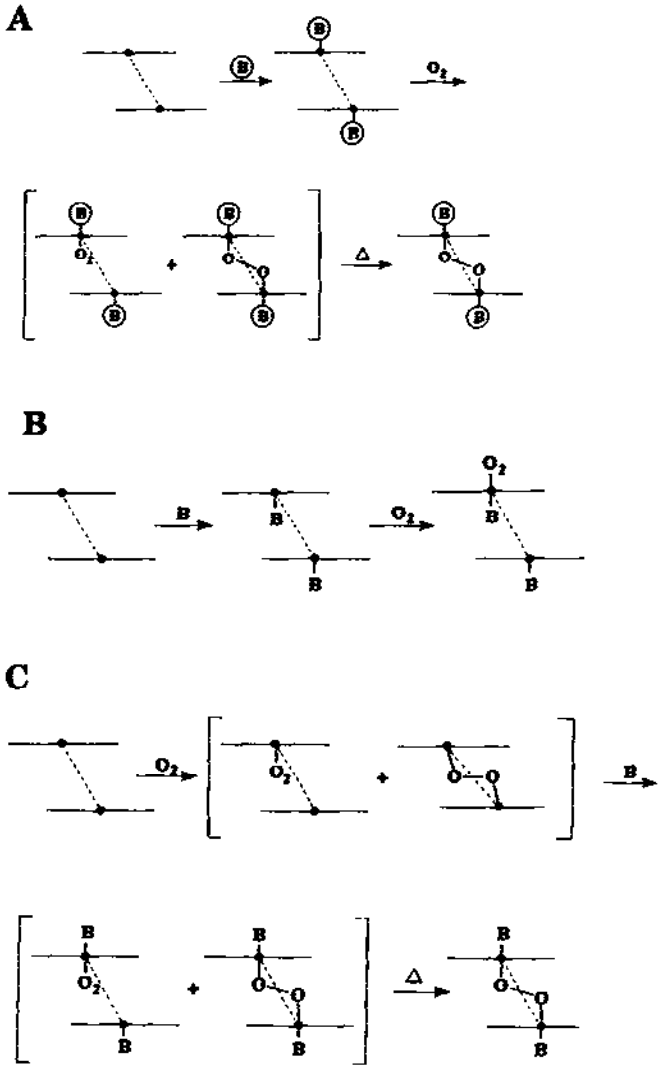

Fig. 18. Reaction schemes: A, large base; B, small base (base added first); C, small base (O_2 added first) [19].

ligand [33]. The observed doublet structure cannot be attributed to the presence of two conformers because a similar doublet structure is not seen in the $\nu(^{18}O_2)$ region (Fig. 19(B)). Previously, Fermi resonance between $\nu(O_2)$ and the first overtone of $\nu(Fe–O_2)$ was invoked to explain the origin of the two oxygen-isotope-sensitive bands (1155 and 1107 cm^{-1}) observed in the IR spectrum of HbO_2 [63]. However, Fermi resonance is not likely to occur in this case because the first overtone of $\nu(Co–O_2)$ ($2 \times 520 = 1040$ cm^{-1}) is

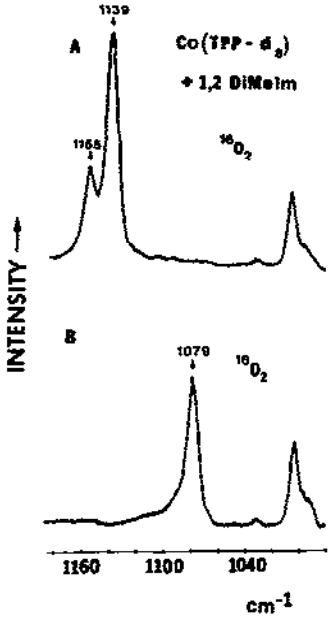

Fig. 19. The RR spectra of Co(TPP-d_8)(1,2-DiMeIm)O_2 (A) and its $^{18}O_2$ analog (B) in CH_2Cl_2 at ca. $-90\,^{\circ}C$ (406.7 nm excitation) [33].

too far from $\nu(O_2)$. The possibility of Fermi resonance between $\nu(O_2)$ and a porphyrin mode is also unlikely because this doublet is observed for other porphyrins whenever 1,2-DiMeIm is used as the base. An extensive study involving a variety of base ligands has shown that such a doublet appears only when the base ligand exhibits an internal mode of the totally symmetric type near 1150 cm^{-1}. Apparently, vibrational coupling between $\nu(O_2)$ and a nearby base-ligand vibration of the same symmetry is responsible for the observed doublet structure and resonance enhancement.

The RR spectrum of Co(TPP-d_8)(py)$^{18}O_2$ in CH_2Cl_2 is shown in Fig. 20(B) [33]. The spectrum shows a strong $\nu(^{18}O_2)$ band at 1084 cm^{-1} and a weak py band at 1067 cm^{-1}. The former band is shifted 2 cm^{-1} to lower frequency and the latter disappears completely when py-d_5 is used instead of py (broken line). The 1067 cm^{-1} band of py is not resonance enhanced in the case of the $^{16}O_2$ adduct (Fig. 20(A)). These results suggest that the appearance of the py band in Fig. 20(B) is due to vibrational coupling between the $\nu(^{18}O_2)$ and py modes at 1067 cm^{-1}.

Thus far we have discussed the vibrational coupling between the $\nu(O_2)$ mode and the internal mode of the base ligand *trans* to dioxygen. However, the internal mode of the solvent molecule can also be resonance enhanced via a similar mechanism. As shown in Fig. 20(A) (solid line), the RR

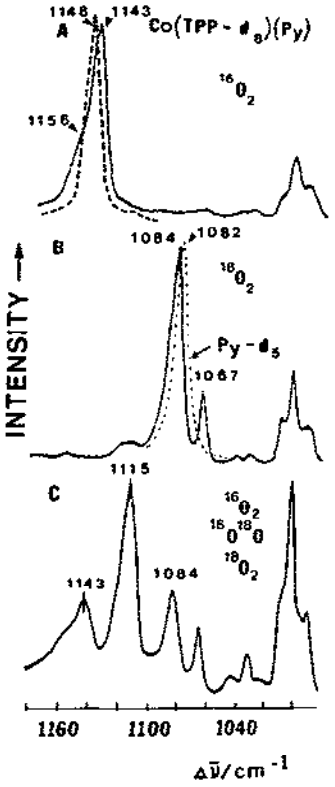

Fig. 20. The RR spectra of Co(TPP-d_8)(py)O_2 in CH_2Cl_2 at ca. $-90\,^{\circ}C$ (406.7 nm excitation) [33]: A, $^{16}O_2$, broken line shows the spectrum in CD_2Cl_2; B, $^{18}O_2$, broken line shows the fragment of the spectrum obtained by using py-d_5 instead of py; C, scrambled dioxygen.

spectrum of Co(TPP-d_8)(py)$^{16}O_2$ in CH_2Cl_2 exhibits the $\nu(^{16}O_2)$ band at 1143 cm^{-1} with a shoulder at ca. 1156 cm^{-1}. In CD_2Cl_2 solution (broken line), this shoulder disappears and the $\nu(^{16}O_2)$ band is shifted to 1148 cm^{-1}. Deuteration of the solvent molecule has no effect on the $\nu(^{18}O_2)$ band. Thus the shoulder at ca. 1156 cm^{-1} must be due to the internal mode of the solvent which is resonance enhanced via vibrational coupling with $\nu(O_2)$.

Figure 20(C) shows the RR spectrum of the same compound obtained with py and scrambled dioxygen ($^{16}O_2 : {}^{16}O^{18}O : {}^{18}O_2 \approx 1:2:1$). The strong band at 1115 cm^{-1} is due to $\nu(^{16}O\text{–}^{18}O)$. Simple diatomic model calculations predict that, if unperturbed, $\nu(^{16}O_2)$ and $\nu(^{18}O_2)$ must be at 1148 cm^{-1} and 1082 cm^{-1} respectively. In fact, these are exactly the same frequencies as those observed in the absence of the vibrational couplings mentioned above. Thus isotope-scrambled spectra provide a sensitive probe for the detection of vibrational coupling.

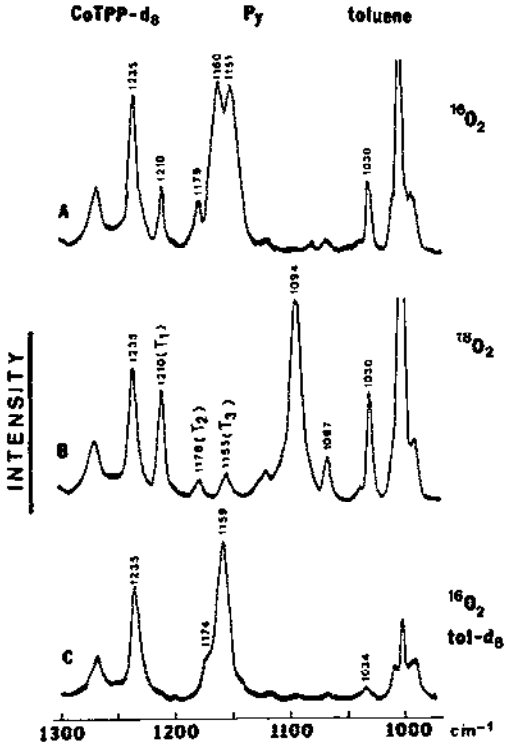

Fig. 21. The RR spectra of Co(TPP-d_8) in toluene containing 3% py at ca. −85 °C (406.7 nm excitation) [46]: A, $^{16}O_2$; B, $^{18}O_2$; C, $^{16}O_2$ (toluene-d_8).

A more dramatic example of vibrational coupling between the $\nu(O_2)$ mode and the internal mode of the solvent is given by the RR spectrum of Co(TPP-d_8)(py)O_2 measured in toluene [46]. As is shown in Fig. 21(A), two strong bands appear at 1160 and 1151 cm^{-1} where the $\nu(^{16}O_2)$ band is expected. This doublet structure is not seen in toluene-d_8 and does not appear in the $\nu(^{18}O_2)$ region (Fig. 21(B)). Toluene exhibits three bands at 1210 cm^{-1} (T_1), 1178 cm^{-1} (T_2) and 1155 cm^{-1} (T_3) with an intensity ratio of ca. 6 : 1 : 1 (Fig. 21(B)). Thus it is reasonable to attribute the observed splitting to a strong coupling between $\nu(^{16}O_2)$ and T_3 which are very close in frequency. If $\nu(^{16}O_2)$ is shifted between T_2 and T_3 by using a weaker base (4-CNpy, Table 3), both internal modes of toluene are resonance enhanced, as can be seen in Fig. 22(A) [46]. In this case, the magnitudes of frequency perturbation and resonance enhancement are less, relative to the previous case, because $\nu(^{16}O_2)$ is further from the solvent modes. As shown in Fig. 22(B), the multiple structure observed for Co(TPP-d_8) disappears completely when cobalt(II) picket-fence porphyrin, Co(T_{piv}, PP), is employed. This result suggests that the vibrational coupling seen for "unpro-

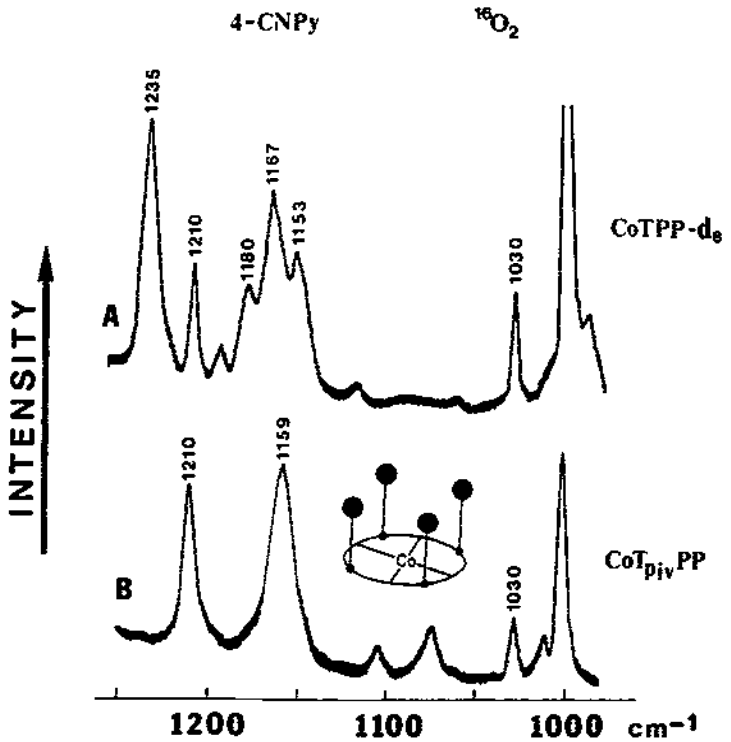

Fig. 22. The RR spectra of Co(TPP-d_8) (A) and Co(T_{piv}PP) (B) in toluene containing 3% 4-CNPy at −85 °C (406.7 nm excitation) [46].

tected" porphyrin cannot occur in picket-fence porphyrin because the four pivaloyl groups prevent the access of toluene to bound dioxygen. Thus not only "frequency matching" but also "direct O_2–solvent association" is necessary to cause such vibrational coupling. The RR spectra of the O_2 adducts of cobalt(II) porphyrins containing 3,5-dichloropyridine as the base have also been analyzed in terms of vibrational coupling between $\nu(O_2)$ and the internal mode of the base ligand or the solvent [64].

G. DIOXYGEN ADDUCTS OF "PROTECTED" PORPHYRINS

Since "unprotected" porphyrins such as Fe(OEP) and Fe(TPP) are rapidly and irreversibly oxidized in air, they are not suited to mimic natural oxygen carriers such as Hb. This oxidation may be prevented by introducing protective groups around the periphery of the porphyrin core. Typical examples of "protected" porphyrins are "picket-fence" [8], "capped" [65], "strapped" [66], "jellyfish" [67] and "hanging-base" [68] porphyrins. Among these porphyrins, the vibrational spectra of the O_2 adducts of picket-fence

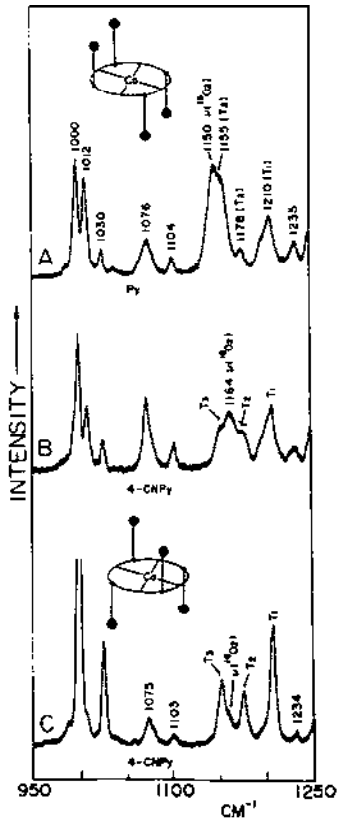

Fig. 23. The RR spectra of Co(*cis*-α^2-T_{piv}PP)(py)O_2 (A), Co(*cis*-α^2-T_{piv}PP)(4-CNPy)O_2 (B) and Co(*trans*-α^2-T_{piv}PP)(4-CNPy)O_2 (C) in toluene at ca. −90 °C (406.7 nm excitation) [15].

porphyrins have been studied most extensively. In Section D, we discussed the effects of metal ion (iron(II) vs. cobalt(II)) and base ligand (N-base vs. thiolate) on the $\nu(O_2)$ and $\nu(M-O_2)$ modes of some picket-fence complexes.

The nature of bound dioxygen inside the picket fence is governed by several factors including the size, shape and polarity of the pocket and by hydrogen bonding between the bound dioxygen and the protic group of the picket fence. In the preceding section, it was shown that the four pickets in the α^4-porphyrin prevent the access of toluene to the bound dioxygen inside the cavity. The RR spectra of Co(*cis*-α^2T_{piv}PP)(py)O_2 and its 4-CNPy derivative in toluene are shown in Figs. 23(A) and 23(B) respectively [15]. In the *cis* structure, direct interaction between O_2 and toluene is possible because there is no steric barrier to prevent such association. As a result, the T_2 mode of toluene is enhanced (Fig. 23(A)). If py is replaced by a weaker base (4-CNPy), $\nu(O_2)$ is shifted to 1164 cm^{-1} and both the T_2 and T_3 modes

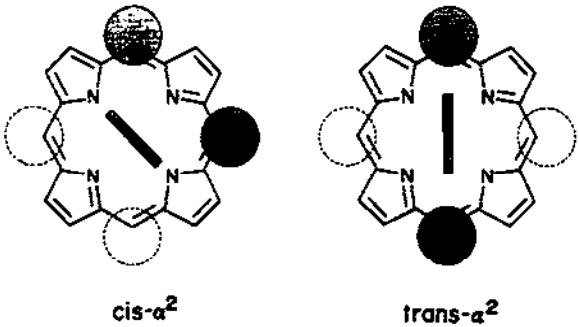

Fig. 24. Schematic representations of relative positions of picket-fence (cross-dotted and open circles above and below the porphyrin core plane respectively) and base ligand plane (dotted rectangular boxes below the porphyrin core plane).

are enhanced (Fig. 23(B)). The RR spectrum of Co(α^3-T_{piv}PP)(4-CNPy)O_2 in toluene is similar to that shown in Fig. 23(B). Evidently, three pickets on one side of the porphyrin plane are not enough to prevent access of the solvent molecule to the dioxygen. Figure 23(C) shows the RR spectrum of Co(*trans*-α^2-T_{piv}PP)(4-CNPy)O_2 in toluene. In this case, the $\nu(O_2)$ band appears as a weak shoulder near the T_3 band. The weakness of $\nu(O_2)$ indicates a low concentration of the O_2 adduct relative to the *cis* isomer.

In "unprotected" porphyrins, the base ligand tends to take the eclipsed orientation with respect to the N_p–Co–N_p (N_p, pyrrole nitrogen) axis of the porphyrin [69]. As shown in Fig. 24, the base ligand is forced to take the eclipsed orientation in the *cis* and the staggered orientation in the *trans* isomer [70]. Thus the degree of π-electron donation from the base to the porphyrin is larger in the *cis* than in the *trans* isomer. This, in turn, would stabilize the O_2 adduct of the *cis* isomer more than that of the *trans* isomer.

Extensive studies on O_2 adducts of "hanging-base" porphyrins [68,71,72] have shown that the bound dioxygen is strongly hydrogen bonded to the amide hydrogen of the "distal" chain (Fig. 25) (N–H $\cdots$ O distance, ca. 3 Å). The presence of a similar but much weaker hydrogen bond (ca. 4 Å) has been proposed for picket-fence porphyrin [73,74]. It was thought [74] that the latter bond is weak because the repulsive force between the $C(CH_3)_3$ group and the bound dioxygen tends to push the pivalamide group outward. The rigid strap structure of hanging-base porphyrin may prevent such a displacement. If the pivalamido group (T_{piv}) is replaced by the neopentylcarboxamido group (T_{neo}) (Fig. 26), this repulsion would be decreased and the N–H $\cdots$ O_2 distance shortened. Thus the $\nu(O_2)$ band is shifted from 1156 to 1148 cm^{-1} in going from Co(α^4-T_{piv}PP)(B)O_2 to its T_{neo}PP analog (B = 4-CNPy) [15]. Further evidence for N–H $\cdots$ O_2 hydrogen bonding is provided by the observation that the ν(Co–O_2) band at 520 cm^{-1} and the

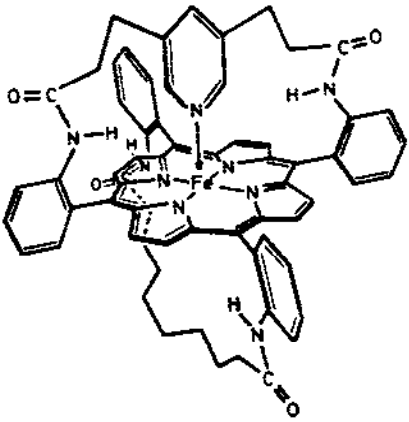

Fig. 25. Structure of "hanging-base" porphyrin [65].

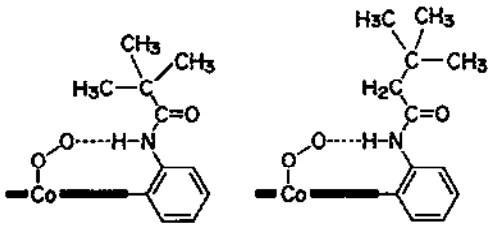

Fig. 26. Hydrogen bonding in $Co(T_{piv}PP)$ and $Co(T_{neo}PP)$ [15].

δ(CoOO) band at 267 cm^{-1} of $Co(\alpha^4\text{-}T_{neo}PP)(4\text{-}PhPy)O_2$ are shifted by 2–3 cm^{-1} to lower frequencies when the NH proton is deuterated [15].

H. NATURALLY OCCURRING DIOXYGEN ADDUCTS

(i) Myoglobin and hemoglobin

Myoglobin (Mb, MW $\approx$ 16000) is an oxygen storage protein found in animal muscles, whereas hemoglobin (Hb, MW $\approx$ 64000) which consists of four subunits (α_1, α_2, β_1 and β_2) is an oxygen transport protein found in animal blood. The active site of these proteins is iron protoporphyrin which is linked to the imidazole nitrogen atom of the proximal histidine (F8) (Fig. 27). In the deoxy state, the iron is divalent and high spin, and the iron atom is out of the porphyrin core plane. Upon oxygenation, dioxygen coordinates to the vacant axial site, and the heme core becomes planar. The iron atom in the oxy state is low spin, and its oxidation state is close to that of iron(III).

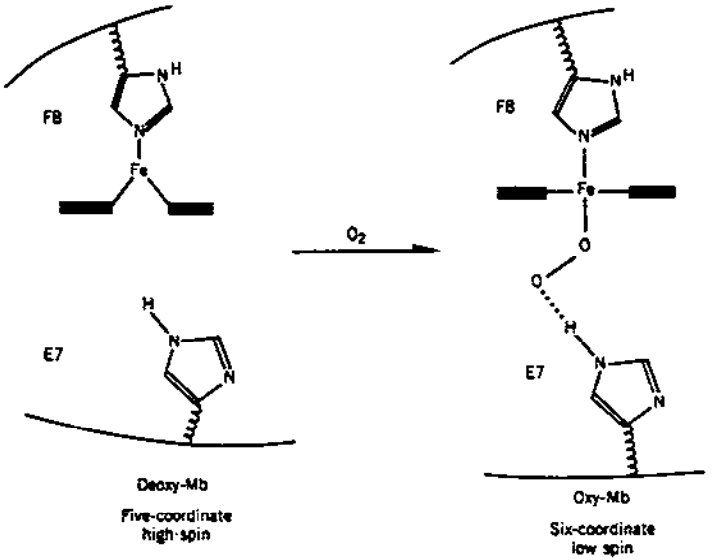

Fig. 27. Active-site structures of deoxy-Mb and oxy-Mb.

Thus six-coordinate "base-bound" dioxygen adducts (Tables 4 and 5) serve as ideal model compounds for these proteins in their oxy states.

Although the $\nu(Fe–O_2)$ band of HbO_2 was located at 567 cm^{-1} by RR spectroscopy (488 nm excitation) [54], attempts to enhance the corresponding $\nu(O_2)$ mode have been unsuccessful, either because of the absence of the $Fe–O_2$ CT transition in the 400–700 nm region, or because its oscillator strength is too small to cause detectable resonance enhancement. Two approaches have been taken to overcome this difficulty. Firstly, the $\nu(O_2)$ region of HbO_2 was measured by IR spectroscopy; it exhibited two oxygen-isotope-sensitive bands of almost equal intensity at 1155 and 1107 cm^{-1} [75], and the origin of this splitting was attributed to Fermi resonance between the unperturbed $\nu(O_2)$ (ca. 1135 cm^{-1}) and the first overtone of $\nu(Fe–O_2)$ at 567 cm^{-1} [63]. Secondly, the RR spectrum of cobalt(II)-reconstituted $HbO_2(CoHbO_2)$ was measured by 406 nm excitation; it exhibited three oxygen-isotope-sensitive bands at 1152 cm^{-1} (weak), 1137 cm^{-1} (strong) and 1107 cm^{-1} (very weak) [55]. The origin of the multiple-band structure was attributed to the presence of two conformers in $CoHbO_2$: conformer **I** is responsible for the bands at 1137 and 1107 cm^{-1}, which result from resonance interaction between the unperturbed $\nu(O_2)$ mode (ca. 1122 cm^{-1}) and the porphyrin mode at 1121 cm^{-1}, while conformer **II** is responsible for the band at 1152 cm^{-1}. According to X-ray analysis of MbO_2 [76], the Fe–O–O plane can take two orientations with respect to the porphyrin plane. In conformer **I**, the Fe–O–O plane is orientated in a

direction which permits the formation of a hydrogen bond between the dioxygen and the NH group of the distal imidazole (E7 in Fig. 27). In conformer **II**, this plane is rotated by 40° from that of conformer **I** so that the dioxygen is free from hydrogen bonding. Thus the $\nu(O_2)$ mode of the latter (1152 cm^{-1}) lies much higher than that of the former (ca. 1122 cm^{-1}). The observed upward shift (2 cm^{-1}) of the 1134 cm^{-1} band of $CoMbO_2$ by H_2O–D_2O (solvent) substitution was regarded as evidence to support the above interpretation [77]. The results of recent IR investigations [78] have also been interpreted on the basis of two conformers which differ in the orientation of the Fe–O–O plane relative to that of the proximal imidazole; conformer **I** exhibits $\nu(O_2)$ at ca. 1125 cm^{-1} which splits into two bands at ca. 1130 cm^{-1} (weak, broad) and ca. 1105 cm^{-1} (strong) cm^{-1} due to an "unidentified" perturbation, while conformer **II** exhibits $\nu(O_2)$ at 1155–1150 cm^{-1} (strong).

Recently, an alternative interpretation has been proposed to explain the origin of the multiple-band structure in the RR spectra of $CoHbO_2$ and $CoMbO_2$ [79]. Namely, these dioxygen adducts exist as a single conformer which exhibits the $\nu(O_2)$ band at ca. 1135 cm^{-1}, and the remaining oxygen-isotope-sensitive bands result from vibrational coupling of $\nu(O_2)$ and the internal modes of the proximal (or possibly distal) imidazole. Evidence to support this interpretation includes the following: (1) the 1153 cm^{-1} band of $CoHbO_2$ disappears completely in D_2O, and a similar band is not seen for $CoMbO_2$ even in H_2O; (2) the difference in $\nu(O_2)$ (ca. 30 cm^{-1}) between the proposed conformers [55] is too large to be attributed to the effect of hydrogen bonding; (3) only a single $\nu(Co–O_2)$ or $\nu(Fe–O_2)$ mode is observed in the low frequency region; and (4) the existence of vibrational coupling between the $\nu(O_2)$ mode and the internal modes of *N*-methylimidazole in model compounds of $CoMbO_2$ and $CoHbO_2$ has been demonstrated. Similar vibrational coupling has been found in the RR spectra of a number of O_2 adducts of cobalt(II) porphyrins (Section D).

The presence of hydrogen bonding between bound O_2 and the distal histidine in MbO_2 (E7, Fig. 27) was first demonstrated by X-ray [76] and neutron diffraction studies [80] which yielded the N–H $\cdots$ O_2 distance of 2.97 Å. This was followed by X-ray analysis of HbO_2 which gave N–H $\cdots$ O_2 distances of 2.7 Å and 3.2–3.4 Å for the α and β subunits respectively [81]. As stated previously, the small upward shift (2 cm^{-1}) in the $\nu(O_2)$ mode of $CoMbO_2$ at 1134 cm^{-1} by H_2O–D_2O substitution [77] was regarded as evidence for such hydrogen bonding. However, the alternative interpretation [79] attributes this shift to changes in vibrational coupling patterns rather than to changes in hydrogen-bond strengths. The latter interpretation, however, does not imply that the N–H $\cdots$ O_2 hydrogen bond is absent in MbO_2 and HbO_2 [79].

(ii) Cytochrome P-450

Cytochromes P-450 (MW ≈ 50 000) are monoxygenase enzymes which catalyze the hydroxylation reaction of substrates such as drugs, steroids, pesticides and carcinogens. The active site of cytochrome P-450 is iron protoporphyrin with the iron center axially bound to the thiolate sulfur of a cysteinyl residue. During the reaction cycle [82], dioxygen is bound to the axial position *trans* to the mercaptide sulfur. This structure is similar to that of HbO_2 except that, in HbO_2, the group *trans* to dioxygen is the imidazole nitrogen of the proximal histidine. In cytochrome P-450, the bound O–O bond is cleaved after one-electron reduction with NADH, and the activated oxygen thus produced or released from the ferryl (Fe=O) porphyrin is utilized for hydroxylation and epoxidation of the substrate. This should be contrasted with Hb which binds dioxygen reversibly without O–O bond cleavage.

As discussed in Section D, the $\nu(O_2)$ mode of $Fe(T_{piv}PP)(1,2\text{-}Me_2Im)O_2$ (1159 cm^{-1}) [8,47] shifts downward by 20 cm^{-1} when the base is replaced by the thiolate ion ($SC_6HF_4^-$) [49] (Table 4). This marked shift was attributed to the effect of lone pair electrons on the sulfur atom, which provide extra electron density to the dioxygen [45]. It was thought [39] that during the reaction cycle of cytochrome P-450 the O–O bond is cleaved under biological conditions because this extra electron density coupled with one-electron reduction with NADH weakens the O–O bond considerably. According to a recent RR study [83], the $\nu(O_2)$ band of oxycytochrome P-450 (camphor-bound) is at 1140 cm^{-1}. This frequency is 15 cm^{-1} lower than that of HbO_2 at 1155 cm^{-1} (IR), which has been assigned to the non-hydrogen-bonded conformer [78].

(iii) Hemerythrins

Hemerythrins (Hr) are non-heme oxygen transport proteins found in invertebrate phyla. Thus far, spectroscopic studies have been focused on Hr isolated from *Golfingia gouldii* (MW = 108 000), which consists of eight subunits. Deoxy-Hr (colorless) turns pink upon oxygenation. The structure of the active site obtained by X-ray analysis [84] is shown in Fig. 28. This structure is markedly different from those of other oxygen transport proteins. The $\nu(O_2)$ and $\nu(Fe\text{–}O_2)$ modes are located at 844 cm^{-1} and 503 cm^{-1} respectively [85]. As expected from the protonated peroxide structure, these bands are shifted by $+4$ cm^{-1} and -3 cm^{-1} respectively in D_2O solution [85]. Such a shift does not occur, however, for the $\nu(O_2)$ mode of $[Fe(III)(E\text{-}DTA)O_2]^-$ at 844 cm^{-1} because the dioxygen takes a side-on structure [86].

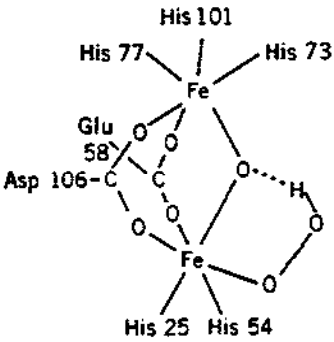

Fig. 28. Active-site structure of oxyhemerythrin [84].

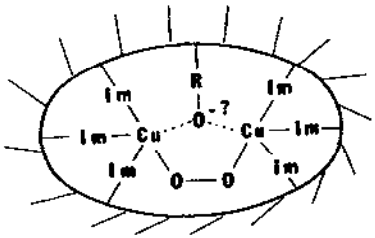

Fig. 29. Proposed active-site structure of oxyhemocyanin [87].

(iv) Hemocyanins

Hemocyanins (Hc) are copper-containing oxygen transport proteins found in the blood of some insects, crustaceans and other invertebrates. One of the smallest Hc (MW ≃ 450000) extracted from spiny lobster (*Panulirus interruptus*) consists of six subunits each containing two copper atoms. The deoxy form (copper(I), colorless) turns blue (copper(II)) upon oxygenation. Figure 29 shows the structure of the active site [87,88]. The $\nu(O_2)$ mode is observed at ca. 750 cm^{-1} which is typical of the peroxo-type adduct [89]. The $\nu(O_2)$ and $\nu(Cu-O)$ modes of its model compound are located at 803 cm^{-1} and 488 cm^{-1} respectively [90].

ACKNOWLEDGEMENTS

The author wishes to express his sincere thanks to all the coworkers who contributed to the research on dioxygen adducts quoted in this review. He is particularly indebted to Professor James R. Kincaid and Dr. Leonard M. Proniewicz who read the manuscript and gave many valuable comments. The National Science Foundation provided continuous financial support for his research on dioxygen adducts.

REFERENCES

1 F. Basolo, B.M. Hoffman and J.A. Ibers, Acc. Chem. Res., 8 (1975) 384.
2 L. Vaska, Acc. Chem. Res., 9 (1976) 175.
3 G. McLendon and A.E. Martell, Coord. Chem. Rev., 19 (1976) 1.
4 R.W. Erskine and B.O. Field, Struct. Bonding, 28 (1976) 1.
5 A.B.P. Lever and H.B. Gray, Acc. Chem. Res., 11 (1978) 348.
6 D.A. Summerville, R.D. Jones, B.M. Hoffman and F. Basolo, J. Chem. Educ., 56 (1979) 157.
7 R.D. Jones, D.A. Summerville and F. Basolo, Chem. Rev., 79 (1979) 139.
8 J.P. Collman, T.R. Halbert and K.S. Suslick, Metal Ion Activation of Dioxygen, Wiley, New York, 1980, p. 1.
9 T.D. Smith and J.R. Pilbrow, Coord. Chem. Rev., 39 (1981) 295.
10 M.H. Gubelman and A.F. Williams, Struct. Bonding, 55 (1983) 1.
11 E.C. Niederhoffer, J.H. Timmons and A.E. Martell, Chem. Rev., 84 (1984) 137.
12 M. Moskowitz and G.A. Ozin, Cryochemistry, Wiley, New York, 1976.
13 H.H. Eysel and S. Thym, Z. Anorg. Allg. Chem., 411 (1975) 97.
14 K. Bajdor, H. Oshio and K. Nakamoto, J. Am. Chem. Soc., 106 (1984) 7273.
15 J. Odo, H. Imai, E. Kyuno and K. Nakamoto, J. Am. Chem. Soc., 110 (1988) 742.
16 T. Shibahara and M. Mori, Bull. Chem. Soc. Jpn., 51 (1978) 1374.
17 C.G. Barraclough, G.A. Lawrence and P.A. Lay, Inorg. Chem., 17 (1978) 3317.
18 I.R. Paeng, H. Shiwaku and K. Nakamoto, J. Am. Chem. Soc., 110 (1988) 1995.
19 L.M. Proniewicz, J. Odo, J. Goral, C.K. Chang and K. Nakamoto, J. Am. Chem. Soc., 111 (1989) 2105.
20 M. Suzuki, T. Ishiguro, M. Kozuka and K. Nakamoto, Inorg. Chem., 20 (1981) 1993.
21 K. Nakamoto, M. Suzuki, T. Ishiguro, M. Kozuka, Y. Nishida and S. Kida, Inorg. Chem., 19 (1980) 2822.
22 S.E. Jacobson, R. Tang and F. Mares, Inorg. Chem., 17 (1978) 3055.
23 M.W. Urban, K. Nakamoto and F. Basolo, Inorg. Chem., 21 (1982) 3406.
24 T. Watanabe, T. Ama and K. Nakamoto, Inorg. Chem., 22 (1983) 2470.
25 E. McCandlish, A.R. Miksztal, M. Nappa, A.Q. Sprenger, J.S. Valentine, J.D. Stong and T.G. Spiro, J. Am. Chem. Soc., 102 (1980) 4268.
26 K. Nakamoto, I.R. Paeng, T. Kuroi, T. Isobe and H. Oshio, J. Mol. Struct., 189 (1988) 293.
27 M. Kozuka and K. Nakamoto, J. Am. Chem. Soc., 103 (1981) 2162.
28 K. Nakamoto, T. Watanabe, T. Ama and M.W. Urban, J. Am. Chem. Soc., 104 (1982) 3744.
29 T. Watanabe, T. Ama and K. Nakamoto, J. Phys. Chem., 88 (1984) 440.
30 K. Nakamoto, Infrared and Raman Spectra of Inorganic and Coordination Compounds, 4th edn., Wiley, New York, 1986, p. 78.
31 T.G. Spiro, Iron Porphyrins, Addison-Wesley, Reading, MA, 1983, Part II, p. 89.
32 K. Nakamoto, Y. Nonaka, T. Ishiguro, M.W. Urban, M. Suzuki, M. Kozuka, Y. Nishida and S. Kida, J. Am. Chem. Soc., 104 (1982) 3386.
33 K. Bajdor, J.R. Kincaid and K. Nakamoto, J. Am. Chem. Soc., 106 (1984) 7741.
34 W. Scheuermann and K. Nakamoto, Appl. Spectrosc., 32 (1978) 251, 302.
35 L.L. Duff, E.H. Appelman, D.F. Shriver and I.M. Klotz, Biochem. Biophys. Res. Commun., 90 (1979) 1098.
36 M.W. Urban, K. Nakamoto and J. Kincaid, Inorg. Chim. Acta, 61 (1983) 77.
37 L. Proniewicz and K. Nakamoto, to be published.

38 L. Proniewicz, T. Isobe and K. Nakamoto, Inorg. Chim. Acta, 155 (1989) 91.
39 K. Bajdor and K. Nakamoto, J. Am. Chem. Soc., 106 (1984) 3045.
40 L.M. Proniewicz, K. Bajdor and K. Nakamoto, J. Phys. Chem., 90 (1986) 1760.
41 S. Hashimoto, Y. Tatsuno and T. Kitagawa, Proc. Jpn. Acad., 60B (1984) 345.
42 A.J. Sitter, C.M. Reczek and J. Terner, J. Biol. Chem., 260 (1985) 7515.
43 K.-J. Paeng and J.R. Kincaid, J. Am. Chem. Soc., 110 (1988) 7913.
44 W.-D. Wagner, I.R. Paeng and K. Nakamoto, J. Am. Chem. Soc., 110 (1988) 5565.
45 K. Nakamoto and H. Oshio, J. Am. Chem. Soc., 107 (1985) 6518.
46 J.R. Kincaid, L.M. Proniewicz, K. Bajdor, A. Bruha and K. Nakamoto, J. Am. Chem. Soc., 107 (1985) 6775.
47 J.P. Collman, J.I. Brauman, T.R. Halbert and K.S. Suslick, Proc. Natl. Acad. Sci. U.S.A., 73 (1976) 3333.
48 G. Chottard, M. Schappacher, L. Richard and R. Weiss, Inorg. Chem., 23 (1984) 4557.
49 M. Schappacher, L. Richard, R. Weiss, R. Montiel-Montoya, E. Bill and A. Trautwein, J. Am. Chem. Soc., 103 (1981) 7646.
50 P. Doppelt and R. Weiss, Nouv. J. Chim., 7 (1983) 341.
51 K. Bajdor, K. Nakamoto and J. Kincaid, J. Am. Chem. Soc., 105 (1983) 678.
52 J.M. Burke, J.R. Kincaid, S. Peters, R.R. Gagne, J.P. Collman and T.G. Spiro, J. Am. Chem. Soc., 100 (1978) 6083.
53 H.C. Mackin, M. Tsubaki and N.-T. Yu, Biophys. J., 41 (1983) 349.
54 H. Brunner, Naturwissenschaften, 61 (1974) 129.
55 M. Tsubaki and N.-T. Yu, Proc. Natl. Acad. Sci. U.S.A., 78 (1981) 3581.
56 A. Dedieu, M.M. Rohmer and A. Veillard, J. Am. Chem. Soc., 98 (1976) 5789.
57 J.E. Newton and M.B. Hall, Inorg. Chem., 23 (1984) 4627.
58 K. Bajdor, K. Nakamoto, H. Kanatomi and I. Murase, Inorg, Chim. Acta, 82 (1984) 207.
59 K. Nakamoto, H. Oshio, H. Okawa, W. Kanda, K. Horiuchi and S. Kida, Inorg. Chim. Acta, 108 (1985) 231.
60 D.−H. Chin, J. Del Gaudio, G.N. La Mar and A.L. Balch, J. Am. Chem. Soc., 99 (1977) 5486.
61 J.M. Burke, J.R. Kincaid and T.G. Spiro, J. Am. Chem. Soc., 100 (1978) 6077.
62 J.A. Hoffman and D.F. Bocian, J. Phys. Chem., 88 (1984) 1472.
63 J.O. Alben, G.H. Bare and P.P. Moh, Biochemical and Clinical Aspects of Hemoglobin Abnormalities, Academic Press, New York, 1978, p. 607.
64 L.M. Proniewicz, K. Nakamoto and J.R. Kincaid, J. Am. Chem. Soc., 110 (1988) 4541.
65 J. Almoz, J.E. Baldwin, R.C. Dyer and J. Peters, J. Am. Chem. Soc., 97 (1975) 226.
66 A.R. Battersby, S.A.J. Bartholemew and T. Nitta, J. Chem. Soc., Chem. Commun., (1983) 1291.
67 Y. Uemori, H. Miyakawa and E. Kyuno, Inorg. Chem., 27 (1988) 377.
68 M. Momenteau and D. Lavalette, J. Chem. Soc., Chem. Commun., (1982) 341.
69 W.R. Scheidt and D.M. Chipman, J. Am. Chem. Soc., 108 (1986) 1163.
70 F.A. Walker, J. Buehler, J.T. West and J.L. Hinds, J. Am. Chem. Soc., 105 (1983) 6923.
71 J. Mispelter, M. Momenteau, D. Lavalette and J.-M. Lhoste, J. Am. Chem. Soc., 105 (1983) 5165.
72 M. Momenteau, Pure Appl. Chem., 58 (1986) 1493.
73 F.A. Walker and J. Bowen, J. Am. Chem. Soc., 107 (1985) 7632.
74 G.B. Jameson and R.S. Drago, J. Am. Chem. Soc., 107 (1985) 3017.
75 W.S. Caughey, M.G. Choc and R.A. Houtchens, Biochemical and Clinical Aspects of Oxygen, Academic Press, New York, 1978, pp. 4 and 18.
76 S.E.V. Phillips, J. Mol. Biol., 142 (1980) 531.

77 T. Kitagawa, M.R. Ondrias, D.L. Rousseau, M. Ikeda-Saito and T. Yonetani, Nature (London), 298 (1982) 869.
78 W.T. Potter, M.P. Tucker, R.A. Houtchens and W.S. Caughey, Biochemistry, 26 (1987) 4699.
79 A. Bruha and J.R. Kindcaid, J. Am. Chem. Soc., 110 (1988) 6006.
80 S.E.V. Phillips and B.P. Schoenborn, Nature (London), 292 (1981) 81.
81 B. Shaanan, Nature (London), 296 (1982) 683.
82 L.S. Alexander and H.M. Goff, J. Chem. Educ., 59 (1982) 179.
83 O. Bangcharoenpaurpong, A.K. Rizos and P.M. Champion, J. Biol. Chem., 261 (1986) 8089.
84 R.E. Stenkamp, L.C. Sieker, L.H. Jensen, J.D. McCallum and J. Sanders-Loehr, Proc. Natl. Acad. Sci. U.S.A., 82 (1985) 713.
85 A.K. Shiemke, T.M. Loehr and J. Sanders-Loehr, J. Am. Chem. Soc., 106 (1984) 4951.
86 S. Ahmad, J.D. McCallum, A.K. Shiemke, E.H. Appelman and T.M. Loehr, Inorg. Chem., 27 (1988) 2230.
87 W.P.J. Gaykema, W.G.J. Hol, J.M. Vereijken, N.M. Soeter, H.J. Bak and J.J. Beintema, Nature (London), 309 (1984) 23.
88 W.P.J. Gaykema, A. Volbeda and W.G.J. Hol, J. Mol. Biol., 187 (1985) 255.
89 T.B. Freedman, J.S. Loehr and T.M. Loehr, J. Am. Chem. Soc., 98 (1976) 2809.
90 J.E. Pate, R.W. Cruse, K.D. Karlin and E.I. Solomon, J. Am. Chem. Soc., 109 (1987) 2624.